Published in final edited form as:

*Cell Stem Cell*. 2023 August 03; 30(8): 1072–1090.e10. doi:10.1016/j.stem.2023.07.001.

# TET2-mediated mRNA demethylation regulates leukemia stem cell homing and self-renewal

**Yangchan Li**[1,5,17], **Meilin Xue**[1,13,17], **Xiaolan Deng**[1,17], **Lei Dong**[1,17], **Le Xuan Truong Nguyen**[2,3], **Lili Ren**[1,14], **Li Han**[1,11], **Chenying Li**[1,15], **Jianhuang Xue**[1], **Zhicong Zhao**[1], **Wei Li**[1], **Ying Qing**[1], **Chao Shen**[1], **Brandon Tan**[1], **Zhenhua Chen**[1], **Keith Leung**[1], **Kitty Wang**[1], **Srividya Swaminathan**[1,12], **Ling Li**[2,3,4], **Mark Wunderlich**[6], **James C. Mulloy**[6], **Xiaobo Li**[14], **Hao Chen**[13], **Bin Zhang**[2,3,4], **David Horne**[4,7], **Steven T. Rosen**[2,4,8], **Guido Marcucci**[2,3,4], **Mingjiang Xu**[9], **Zejuan Li**[10], **Minjie Wei**[11], **Jingyan Tian**[16,*], **Baiyong Shen**[13,*], **Rui Su**[1,4,*], **Jianjun Chen**[1,2,4,18,*]

[1]Department of Systems Biology, Beckman Research Institute of City of Hope, Monrovia, CA 91016, USA

[2]Gehr Family Center for Leukemia Research, City of Hope, Duarte, CA 91010, USA

[3]Department of Hematological Malignancies Translational Science, Beckman Research Institute of City of Hope, Monrovia, CA 91016, USA

[4]City of Hope Comprehensive Cancer Center, Duarte, CA 91010, USA

[5]Department of Radiation Oncology, The First Affiliated Hospital of Sun Yat-sen University, Guangzhou, Guangdong 510080, China

[6]Division of Experimental Hematology and Cancer Biology, Cincinnati Children's Hospital Medical Center, Cincinnati, OH 45229, USA

[7]Department of Molecular Medicine, Beckman Research Institute of City of Hope, Duarte, CA 91010, USA

[8]Department of Hematology/Hematopoietic Cell Transplantation, City of Hope, Duarte, CA 91010, USA.

[9]Department of Molecular Medicine, University of Texas Health San Antonio, San Antonio, TX 78229, USA

[*]Correspondence: tianjypaper@163.com (J.T.); shenby@shsmu.edu.cn (B.S); rsu@coh.org (R. S.); jianchen@coh.org (J. C.).

Author Contributions

R.S. and J.C. conceived and designed the entire project, and supervised the research conducted in their laboratories; Y.L., M.X., X.D., L.S.T.N., L.R., L.H., C.L., J.X., Z.Z., W.L., Y.Q., C.S., B.T., M.X., K.L., K.W., R.S., and J.C. performed experiments and/or data analyses; L.D. performed the bioinformatics analysis; S.S., L.L., M.W., J.M., X.L., H. C., B.Z., D.H., S.T.R., G.M., Z.L., M.W., J.T., B.S., R.S., and J.C. contributed reagents/analytic tools and/or grant support; Y.L., M.X., X.D., L.D., R.S., and J.C. wrote the paper. All authors discussed the results and commented on the manuscript.

Declaration of interests

The authors declare no competing interests.

[10]Department of Pathology and Genomic Medicine, Houston Methodist Hospital, Houston, Texas, USA.

[11]Department of Pharmacology, School of Pharmacy, China Medical University, Shenyang, Liaoning 110001, China

[12]Department of Pediatrics, Beckman Research Institute of City of Hope, Duarte, CA91010, USA

[13]Department of General Surgery, Pancreatic Disease Center, Ruijin Hospital, Shanghai Jiao Tong University School of Medicine, Shanghai 200025, China

[14]Department of Pathology, Harbin Medical University, Harbin 150081, China

[15]Department of Hematology, the First Affiliated Hospital, Zhejiang University School of Medicine, Hangzhou, Zhejiang 31003, China

[16]State Key Laboratory of Medical Genomics, Clinical Trial Center, Shanghai Institute of Endocrine and Metabolic Diseases, Department of Endocrinology and Metabolism, Ruijin Hospital, Shanghai Jiao Tong University School of Medicine, Shanghai, 200025 China

[17]These authors contributed equally

[18]Lead Contact

## Summary

TET2 is recurrently mutated in acute myeloid leukemia (AML) and its deficiency promotes leukemogenesis (driven by aggressive oncogenic mutations) and enhances leukemia stem cell (LSC) self-renewal. However, the underlying cellular/molecular mechanisms have yet to be fully understood. Here we show that *Tet2* deficiency significantly facilitates leukemogenesis in various AML models (mediated by aggressive or less aggressive mutations) through promoting homing of LSCs into bone marrow (BM) niche to increase their self-renewal/proliferation. TET2 deficiency in AML blast cells increases expression of Tetraspanin 13 (TSPAN13) and thereby activates the CXCR4/CXCL12 signaling, leading to increased homing/migration of LSCs into BM niche. Mechanistically, TET2 deficiency results in the accumulation of methyl-5-cytosine ($m^5C$) modification in *TSPAN13* mRNA; YBX1 specifically recognizes the $m^5C$ modification and increases the stability and expression of *TSPAN13* transcripts. Collectively, our studies reveal the functional importance of TET2 in leukemogenesis, leukemic blast cell migration/homing, and LSC self-renewal as an mRNA $m^5C$ demethylase.

## In Brief

Li and colleagues report that *TET2* deficiency facilitates LSC homing into bone marrow microenvironment, giving rise to increased LSC self-renewal and fast leukemogenesis in various animal models. Mechanistically, *TET2* deficiency enhances the stability of *TSPAN13* mRNA as an mRNA $m^5C$ demethylase and thereby triggers the CXCR4/CXCL12 signaling.

## Graphical Abstract

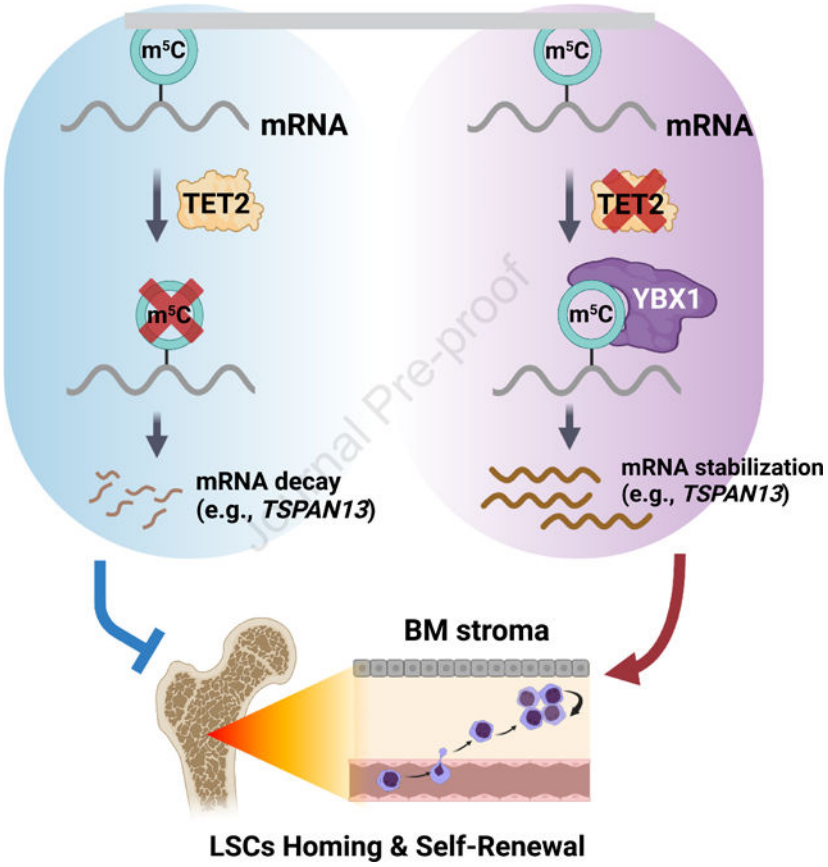




## Introduction

In the normal hematopoietic system, gene expression is strictly orchestrated not only by genetic enhancers and promoters, but also by epigenetic and epitranscriptomic modifications. Evidence is emerging that the dysregulation of covalent chemical modifications in DNA or RNA leads to hematopoietic malignancies, including acute myeloid leukemia (AML) [1–4]. For instance, somatic depletions and loss-of-function mutations of tet methylcytosine dioxygenase 2 (TET2) have been characterized in 15–20% of AML, 30% of myelodysplastic syndrome (MDS), and 50% of chronic myelomonocytic leukemia (CMML) cases [5–7]. TET2 catalyzes the conversion of 5-methylcytosine (5mC) to 5-hydroxy/formyl/carboxyl-cytosine (5hmC, 5fC, 5caC) to mediate DNA demethylation and plays a central role in regulating gene expression at the transcriptional level [8–10]. The vast majority of TET2 mutations lose demethylation activity and have been recognized as the initial step of myeloid malignant transformation in AML [4,11]. Moreover, *TET2* deficiency confers poor prognosis and drug resistance in AML patients [12–16]. In addition to oxidization of DNA 5mC modification, recent studies support a novel function for TET2-mediated demethylation of methyl-5-cytosine (termed as 'm$^5$C' to distinguish from DNA 5mC) in RNAs, including messenger RNAs (mRNAs) [17–20]. However, the systemic investigation of the role and biological relevance of mRNA m$^5$C is still in its infancy [21–23]. It is completely

unknown whether and (if so) how TET2-induced mRNA $m^5C$ demethylation contributes to leukemogenesis or tumorigenesis in general.

AML, one of the most common and aggressive types of blood malignancies, is featured by the clonal expansion of immature leukemia stem cells (LSCs). Despite currently available treatments, over 70% of AML patients do not survive over 5 years [24,25]. Relapse remains the principal cause of treatment failure and occurs in over 50% of AML patients [26]. LSCs are at the apex of the AML cellular hierarchy and are considered the root cause of drug resistance and AML relapse [27–29]. Thus, eradicating LSCs is critical in curing AML. LSCs reside in specialized microenvironments called “niches” in the bone marrow (BM) to support their survival and maintain their self-renewal capacity [30]. It was known that the direct interplay between the chemokine receptor 4 (CXCR4) and its ligand CXCL12 (also called stromal cell-derived factor-1, SDF-1) primes the crosstalk between LSCs and BM stromal cells in the microenvironment [31]. Pharmacological inhibition of CXCR4 prevents the anchorage of AML cells and promotes the mobilization of LSCs out of the endosteal niche, thereby improving their vulnerability to chemotherapy agents [32].

The function of TET2 in hematopoietic differentiation and LSC maintenance has been well documented [6,11,14,33–35], but the underlying cellular/molecular mechanisms remain largely elusive. Although previous studies suggested that TET2 deficiency facititated leukemogenesis driven by aggressive mutations such as MLL-AF9 and AML1-ETO9a [36,37], the impact of TET2 deficiency on other AML models driven by less aggressive mutations has yet to be determined. Moreover, the roles of TET2 in BM microenvironment/niche programming have yet to be investigated. Here we show that TET2 functions as RNA demethylase, mediating the post-transcriptional regulation of *tetraspanin 13* (*Tspan13*) mRNA stability. As a result, *Tet2* deficiency causes the activation of the Tspan13/Cxcr4 axis, which in turn leads to increased LSC homing/self-renewal, thereby promoting leukemogenesis. Overall, our studies uncover previously unappreciated roles and underlying molecular mechanisms of TET2 in regulating BM niche programming and LSC homing/self-renewal in AML pathogenesis, as an RNA demethylase.

## Results

### Decreased expression or deficiency of *TET2* is associated with poor prognosis in AML patients

Given that previous studies predominantly focus on loss-of-function mutations of TET2, we tried to analyze the overall expression level of TET2 and its clinical relevance in AML. In the analysis of The Cancer Genome Atlas (TCGA) AML cohort, we found that lower expression of *TET2* transcript is significantly correlated with shorter survival in AML patients (Figure 1A). TET2 expression is significantly suppressed in AML patients, including those carrying t(15;17), t(8;21), MLL-rearrangement (MLL-r)/t(11q23), and normal karyotype, relative to healthy controls (Figure 1B) [38]. Moreover, the expression of TET2 as well as TET3, but not TET1, is also decreased in adverse-risk AML patients relative to the patients with favorable-risk AMLs [39] (Figures 1C and S1A–S1B). Thus, a lower expression level of TET2 is significantly associated with a poor prognosis in AML patients. Similarly, AML patients with TET2 loss-of-function mutations are also

associated with shorter overall survival compared to patients with wildtype TET2 (Figure 1D). Notably, TET2 mutations frequently co-occurred with the mutations in other genes such as FLT3, DNMT3A, NPM1, and RAS, as well as translocations such as t(11q23)/MLL-rearrangements and t(8;21)/RUNX1-RUNXT1 in AML patients (Figures S1C–S1D). Furthermore, single-cell RNA-seq data from AML patients [40] indicates that expression level of *TET2* is significantly lower in primitive (immature) AML cell population compared to the relatively mature (differentiated) AML cell population (Figure S1E). In addition, TET2, but not TET1 or TET3, is expressed at a significantly lower level in normal hematopoietic stem/progenitor cells (HSPCs) relative to normal mature myeloid cells (Figures S1F–S1G). Such data suggest that TET2 might be required for the differentiation of HSPCs and LSCs.

### *Tet2* deficiency induces rapid primary leukemogenesis

To further evaluate the role of Tet2 in primary leukemogenesis, we have generated various AML models driven by AML1-ETO9a (AE9a, resulting from t(8;21) translocation) [41], MLL-AF9 (MA9, MLL-r/t(11q23)), PML-RARA (t(15;17) translocation), NRAS mutation, $FLT3^{ITD}$, and DNMT3A mutation, coupled with $Tet2^{+/+}$ and $Tet2^{-/-}$ mouse models (Figure 1E). Such selection is clinically relevant because TET2 mutation and/or transcriptional suppression have been characterized in those AML subtypes (see Figures 1B and S1C–S1D). Notably, *Tet2* depletion dramatically promoted primary leukemogenesis in the BM transplantation (BMT) recipient mice (Figures 1F–1H and S1H). Furthermore, *Tet2* depletion exacerbated leukocytosis, anemia, and thrombocytopenia (Figures 1I–1K) in peripheral blood (PB) of the recipient mice. *Tet2* deficiency also led to splenomegaly, increased white blood cell (WBC) count, and a significant increase in the engraftment of primary AML cells into PB, BM, and spleen (Figures 1L–1P and S1I–S1L). Histopathology demonstrated the heavier infiltration of $Tet2^{-/-}$-leukemic blasts into spleen and liver, which disrupted their normal architecture (Figures S1M and S1N). Wright-Giemsa staining of PB and BM revealed the notably larger and less differentiated blasts in the *Tet2*-deficient cohorts compared to the $Tet2^{+/+}$ counterparts (Figures S1M). Via flow cytometry, we verified that *Tet2* deficiency significantly attenuated myeloid differentiation in primary AML cells (Figures S1O–S1P).

### *Tet2* deficiency enhances LSC self-renewal

To decipher the mechanism(s) by which *Tet2* deficiency dramatically promotes leukemogenesis *in vivo*, we collected primary $Tet2^{-/-}$ and $Tet2^{+/+}$ AML cells for RNA-seq analysis. We found that *Tet2* deficiency significantly increased expression of the genes enriched in the “Hematopoiesis Stem Cell” pathway (Figures 2A–2B). To validate whether *Tet2* deletion impacts the self-renewal of LSCs, we conducted *in vitro* colony-forming/re-plating assay. More colonies with larger sizes and more cells were observed in *Tet2* deficient pre-LSCs transduced with NRAS/AE9a in the serial replating assay (Figures 2C and S2A–S2B). Meanwhile, we analyzed the percentage of LSCs ($Lin^-c\text{-}Kit^+Sca\text{-}1^+$, LSK) by flow cytometry (Figure S2C). As expected, *Tet2* deficiency in NRAS/AE9a transformed pre-leukemic cells led to a significant increase in the $Lin^-$ and LSC subpopulations, especially after 3 rounds of replating (Figure S2D and 2D). Consistently, we verified that *Tet2* deficiency attenuated myeloid differentiation of the pre-leukemic cells via checking myeloid differentiation markers Gr-1 and Mac-1 (Figure S2E). In the MA9-driven pre-AML model,

*Tet2* deficiency also resulted in an increase in $Lin^-$ and LSC subpopulations (Figure S2F–S2G). Consistently, *Tet2* deficiency significantly potentiated the colony-forming/replating ability in additional pre-AML models driven by $FLT3^{ITD}$, DNMT3A-mutant/NRAS-mutant, DNMT3A-mutant/ $FLT3^{ITD}$, or NRAS-mutant/PML-RARA (Figures 2E–2F and S2H).

To assess the impact of *Tet2* depletion on LSC self-renewal *in vivo*, we performed secondary BMT. We found that *Tet2*-deficient MA9 leukemic cells showed a dramatically higher engraftment/expansion in BM (Figure S3A) and developed AML with much shorter latency (Figure 2G) than did the *Tet2*-wildtype counterparts, accompanied by a significant increase in WBC count (in PB) as well as spleen size and weight (Figures 2H and S3B–3C). We next conducted *in vivo* limiting dilution assay (LDA) to quantitatively assess the effect of *Tet2* deficiency on LSC self-renewal capability. Remarkably, *Tet2* deletion significantly increased LSCs frequency in MA9 AML model by over 30-fold (Figure 2I). We further confirmed the robust impact of *Tet2* depletion on LSC frequency in NRAS/AE9a- and NRAS/PML-RARA-transformed pre-leukemic cells as detected by *in vitro* LDA assays (Figures S3D–S3F). In addition, we determined the percentages of the $Lin^-$ c-$Kit^+Sca\text{-}1^-CD34^+Fc\gamma RII/III^+$ granulocyte-macrophage progenitor-like (L-GMP; representing LSC population in MA9-induced AML[42]) cells as well as differentiated myeloid cells in the BM of primary recipient mice of the MA9 AML model (Figure S3G). We showed that *Tet2* deficiency evidently increased the undifferentiated L-GMP population and substantially decreased the differentiated ($Gr\text{-}1^+Mac\text{-}1^+$) cell population (Figures S3H–S3J). Altogether, our data demonstrate that *TET2* loss increases LSC self-renewal and suppresses myeloid differentiation *in vitro* and *in vivo* in various murine AML models.

## *TET2* overexpression suppresses human AML blast cell repopulation and inhibits AML progression *in vivo*

Consistent with the suppressive role of Tet2 in murine LSC self-renewal, the expression level of TET2 is also significantly lower in human $CD34^+$ primitive AML blasts compared to the $CD34^-$ bulk AML cells (Figures 2J–2K). Moreover, forced expression of TET2 dramatically decreased the colony-forming/replating ability of primary AML PDX cells and Mono Mac 6 AML cells (Figures 2L–2N), implying that TET2 may also play a suppressive role in human AML repopulation and progression. To evaluate the *in vivo* role of TET2 in AML in a setting relevant to human disease, we utilized patient-derived xenograft (PDX) and ‘human-in-mouse’ xenograft AML models. As expected, forced expression of TET2 in AML PDX cells (isolated from a relapsed patient) significantly suppressed AML blast cell repopulation, decreased leukemia burden and improved the overall survival in recipient mice (Figures 2O–2Q and S3K). Consistently, overexpression of TET2 in Mono Mac 6 AML cells (carrying MA9 translocation) significantly mitigated splenomegaly, decreased WBC number, suppressed engraftment into spleen and BM of NRGS mice, and substantially prolonged their survival (Figures 2R and S3L–S3P). Collectively, our studies have demonstrated that TET2 plays a potent tumor-suppressive role in various human and murine AML models, in which TET2 suppresses the self-renewal/repopulation of AML blast cells or LSCs.

### *Tet2* deficiency accelerates LSC homing/migration *in vitro*

To determine whether *Tet2* deficiency offered a profound growth advantage to facilitate rapid and aggressive leukemogenesis, we analyzed the effects of Tet2 deficiency on the growth/proliferation and cell cycle of primary AML cells *in vitro*. Strikingly, *Tet2* depletion had very weak effects on the growth/proliferation and cell cycle of primary AML cells in liquid culture (Figures S4A–S4E). In contrast, when co-cultured with stroma cells, $Tet2^{-/-}$ AML cells substantially outperformed $Tet2^{+/+}$ AML cells in proliferation/growth (Figures 3A–3D), implying that the microenvironment plays a pivotal role in regulating *Tet2* deficiency-mediated rapid leukemogenesis *in vivo*.

Considering that LSCs reside in the BM niche, which plays an essential role in maintaining LSC self-renewal ability, we sought to investigate the effect of *Tet2* deficiency on LSC homing to BM microenvironment and on LSC frequency. Through *in vitro* LDA assays, we showed that *Tet2* loss significantly increased LSC frequency in the single culture system, while co-culture of LSCs, particularly the *Tet2*-deficient LSCs, with stroma cells substantially potentiated their self-renewal ability (Figures 3E–3G). Additionally, employing the transwell assay, we found that *Tet2/TET2* loss significantly promoted the migration of various types of murine and human AML cells into stromal cells (Figures 3H–3L). Collectively, our results suggest that *TET2* deficiency can promote LSC homing/migration to stromal cells and subsequently increase LSC self-renewal *in vitro*.

### *Tet2* deficiency facilitates homing of LSCs *in vivo*

During BMT, the homing and/or anchoring of LSC into the BM niche plays a predominant role to maintain/enhance LSC self-renewal *in vivo*. We employed the *in situ* confocal immunofluorescence (IF) imaging and flow cytometry (Figure 4A) to investigate whether *Tet2* deficiency-induced LSC self-renewal was due to the increased migration into BM niche. Osteopontin (OPN), an extracellular molecule secreted by osteoblast, can anchor LSCs to support their survival and self-renewal in BM microenvironment [43] and represent the stem cell niche in the BM. Our *in situ* staining data showed that there were significantly more *Tet2* deficient-AML cells migrating into the $OPN^{+}$ BM-derived stromal cells relative to the *Tet2* wildtype group (Figures 4B–4C). By flow cytometry, we further validated that *Tet2* deficiency indeed enhanced the homing of primary MA9 AML cells (Figures 4D and S5A). Furthermore, we collected the samples at various time points (1, 4, 12, and 16 hours) to carefully evaluate the effect of *Tet2* deficiency on the homing of AML blasts (i.e., immature AML cells, including LSCs). We were able to detect significantly increased homing of *Tet2*-deficient AML blasts starting at around 12 hours post-transplantation (Figures 4E and S5B). In the NRAS/AE9a-driven primary AML models and MA9-driven secondary AML models, *Tet2* deficiency also significantly enhanced homing of AML blasts (Figures 4F–4G and S5C). Conversely, overexpression of TET2 in AML PDX cells substantially attenuated their homing into the BM of NRGS mice (Figure 4H). In the BM niche, AML blasts, particularly LSCs, are surrounded by various stromal cells which support their stemness and self-renewal ability [31]. Our data suggest that co-culture with stroma cells notably increases the migration/homing, proliferation, and self-renewal ability of *Tet2*-deficient AML cells (see Figures 3E–3L and 3A–3D). Therefore, the increased

migration and homing of primary AML cells into BM niche might be a major contributor to *Tet2* deficiency-induced rapid and aggressive leukemogenesis *in vivo*.

## Tspan13 is responsible for *Tet2* deficiency-enhanced LSC homing and self-renewal

To dissect the mechanism(s) by which *Tet2* depletion promotes LSC homing and self-renewal, we performed RNA-seq using two *Tet2* knockout (KO) models. One model lacked exons 8 to 10 [44] (see Figure 2B), and the other lacked exon 3 [11] (Figure S6A). In line with the $Tet2^{-/-}$ (ΔE8–10) NRAS/AE9a AML model, deletion of exon 3 ($Tet2^{-/-}$ (Δ3)) also dramatically increased expression of the genes associated with hematopoiesis stem cell signature in the NRAS/AE9a AML model (Figure S6B). Amongst all the core-enriched genes of stem cell pathways in the two $Tet2^{-/-}$ NRAS/AE9a AML models, we identified 41 overlapped potential targets (Figures 5A–5B and S6C). Furthermore, we analyzed the expression correlation between *TET2* and the 41 co-enriched genes in 3 distinct AML cohorts. We identified that only *TSPAN13* and *synaptic vesicle glycoprotein 2A* (*SV2A*) exhibited a significantly negative correlation with *TET2* in all the 3 human AML cohort datasets (Figures 5C and S6D–S6E). *TSPAN13*, but not *SV2A*, is expressed at a significantly higher level in patients with adverse-risk AML than in patients with favorable-risk AML prognosis (Figures 5D–5E), in an expected pattern opposite to that of *TET2* (see Figure 1C). *Tet2* deficiency-mediated upregulation of *Tspan13* was confirmed in primary murine AML cells by RNA-seq and qPCR (Figures 5F–5G). TSPAN13 belongs to the tetraspanin family, which is implicated in adhesion, trafficking, and cell signaling within the niche of hematopoietic stem cells (HSCs) and LSCs [45–48]. To evaluate the functional involvement of TSPAN13 in AML pathogenesis, we used a lentiviral vector-based short hairpin RNA (shRNA) system to knock down the expression of *Tspan13* (sh1 and sh2) in *Tet2*-deficient primary AML cells (Figure 5G). Depletion of *Tspan13* significantly decreased the colony-forming ability of *Tet2*-deficient AML blasts (Figures 5H–5J). LDAs demonstrated that *Tspan13* KD significantly decreased LSC frequencies in AML blasts (Figures S6F–S6G). Furthermore, *Tspan13* depletion not only attenuated the LSC homing into the BM niche (Figure S6H–S6I) but also almost completely reversed the enhanced LSC homing in the BM microenvironment caused by *Tet2*-deficiency (Figured 5K). Additionally, genetic depletion of *Tspan13* substantially reversed *Tet2* deficiency-enhanced LSC self-renewal (Figure 5L). We also conducted BMT to define whether *Tspan13* was required for AML development *in vivo* and showed that *Tspan13* depletion dramatically inhibited AML progression driven by *Tet2*-deficient primary AML cells and led to a significantly prolonged overall survival (Figure 5M) and dramatically suppressed engraftment of primary AML cells in the recipient mice (Figure 5N). Altogether, our data suggest that *Tspan13* is a functionally essential target of *Tet2*, and the upregulation of *Tspan13* is necessary for *Tet2*-deficiency enhanced AML pathogenesis and LSC homing and self-renewal.

## *Tet2* depletion activates the Tspan13/Cxcr4/Cxcl12 signaling to facilitate LSC homing

Considering that *Tet2* deficiency-induced upregulation of Tspan13 is responsible for LSC homing, our following question was how *Tspan13* influenced AML homing. The interaction between CXCR4 and CXCL12 was reported to be fundamental for LSC homing [49,50], and multiple members in the Tetraspanin family, such as *TSPAN3, TSPAN29,* and *TSPAN30*, have been reported to regulate CXCR4 expression to modulate cell migration, adhesion,

and homing [46,51,52]. We therefore checked the expression levels of the activated (Ser339 phosphorylated) Cxcr4 (p-Cxcr4) in both murine and human primary AML cells upon *Tet2*/*TET2* depletion and overexpression. Our results showed that *Tet2* deficiency potentiated Cxcr4 activation (Figure 6A), while forced expression of TET2 suppressed the activation of CXCR4 (Figure 6B). Furthermore, we checked the surface expression of activated Cxcr4 via flow cytometry and showed that *Tet2* deficiency significantly increased the expression of surface p-Cxcr4 (Figure 6C), while depletion of *Tspan13* dramatically decreased its surface expression (Figure 6D). To further verify our discovery that *Tet2* deficiency-mediated LSC homing is attributed to the activation of the Cxcr4/Cxcl12 axis, we pre-treated stromal cells with a neutralizing antibody against Cxcl12 to block Cxcl12-induced chemotaxis and then co-cultured them with AML cells (Figure 6E). Pretreatment with Cxcl12 antibody could largely reverse *Tet2* deficiency-induced AML migration (Figure 6F). Moreover, *Tspan13* depletion-mediated inhibition of *Tet2*-deficient LSC migration was comparable to the trend mediated by Cxcl12 antibody (Figure 6G). Furthermore, we pretreated AML blasts with Cxcr4 inhibitor (Cxcr4i, AMD3100) to evaluate whether the Cxcr4/Cxcl12 axis was responsible for *Tet2* deficiency-mediated LSC homing *in vivo* (Figure 6H). As shown in Figures 6I and 6J, inhibition of Cxcr4 could substantially reverse *Tet2* deficiency-enhanced LSC homing *in vivo*. Therefore, our results demonstrate that *Tet2* deficiency facilitates LSC homing mainly through activating the Tspan13/Cxcr4/Cxcl12 axis.

## TET2 negatively regulates *TSPAN13* expression via mRNA oxidation

Next, we sought to delineate the underlying mechanism by which *TET2* depletion promotes the expression of *TSPAN13* (Figure 7A). We first evaluated the transcription efficiency of Tspan13 in $Tet2^{+/+}$ and $Tet2^{-/-}$ primary AML cells, because *Tet2*-mediated DNA demethylation usually regulates gene expression at the transcriptional level [53]. Surprisingly, the transcription efficiency of *Tspan13* was not elevated by *Tet2* depletion as detected by the nuclear Run-on assay (Figures 7B and S7A), and the DNA 5hmC abundance of *Tspan13* was not significantly influenced by *Tet2* depletion either (Figure S7B), suggesting that *Tet2* deficiency-mediated upregulation of *Tspan13* is not dependent on DNA demethylation or transcriptional regulation. Recently, evidence is emerging that TET2 also exerts a novel biological function to fine-tune gene expression at the post-transcriptional level by inducing RNA $m^5C$ oxidization as an mRNA demethylase [17–20]. We thus assessed the potential effect of *Tet2* depletion on the stability of *Tspan13* mRNA. We found that *Tet2* deficiency indeed significantly elongated the half-life of *Tspan13* transcript in AML cells (Figures 7C and S7C–S7D).

To determine whether the effect of *TET2* depletion on the stability of *TSPAN13* mRNA is caused by TET2-mediated oxidation of $m^5C$ (into $hm^5C$) in *TSPAN13* mRNA, we first established the QQQ-MS method to quantitively and precisely determine the abundance of both $m^5C$ and $hm^5C$ (Figure 7D). Next, we conducted an in *vitro* (cell-free) demethylation assay with $m^5C$-modified single-stranded RNA (ssRNA) and purified TET2 protein (Figure S7E). The 5mC-modified DNA was also included as a positive control. Our results confirmed that TET2 could catalyze the formation of both $hm^5C$ in RNA and 5hmC in DNA (Figures S7F–S7G). Furthermore, we employed the *in vitro* demethylation assay with $m^5C$-modified *TSPAN13* mRNA and TET2 protein, and verified that TET2 could

remove the methyl group from $m^5C$ modification in *TSPAN13* mRNA as detected by both QQQ-MS and dot blot assays (Figures 7E–7G). Distinct from the abundant 5hmC in DNA, the endogenous $hm^5C$ level in mRNA in cells is much lower, even below the limit of QQQ-MS detection (Figure S7H), consistent with previous reports [17,54]. Therefore, we mainly focused on the $m^5C$ decoration in mRNA. In the primary AML cells, *Tet2* deficiency significantly increased global $m^5C$ abundance in poly(A) RNA (Figures 7H–7I), the opposite was true when we ectopically expressed *Tet2* (Figure S7I). More specifically, we conducted gene-specific $m^5C$ qPCR to determine the $m^5C$ level in *Tspan13* transcript and demonstrated that *Tet2* loss significantly increased the $m^5C$ abundance in *Tspan13* mRNA (Figure 7J). Moreover, Tet2 protein, either the catalytic domain (CD) or the full length, directly interacted with *Tspan13* mRNA *in cellulo* (Figures 7K and S7J–S7M).

A recent study revealed that Ybx1 functions as an $m^5C$ reader and stabilizes the $m^5C$-modified mRNA [55]. To evaluate whether Ybx1 was required to regulate *Tspan13* mRNA stability via recognizing $m^5C$ residue, we first conducted CLIP-qPCR to determine whether Ybx1 could directly interact with *Tspan13* mRNA. As expected, Ybx1 directly bound with the *Tspan1*3 transcript (Figures 7L and S7N–S7O). In addition, genetic depletion of *Ybx1* significantly accelerated the degradation of *Tspan13* mRNA (Figures 7M and S7P). Finally, we conducted mRNA bisulfite sequencing and stability profiling to assess the effect of *Tet2* deficiency on mRNA $m^5C$ modification and stability, respectively, at the whole transcriptome level. The mRNA bisulfite sequencing showed that *Tet2* deficiency in primary AML cells led to a gain of $m^5C$ sites in over 7,000 transcripts (Figures S7Q–S7R). Moreover, the mRNA half-time profiling showed that *Tet2* deficiency resulted in a global increase of mRNA stabilities (Figure 7N). Specifically, *Tet2* deficiency led to a significant increase of half-time of 1,347 transcripts (Figure 7O), and most of those transcripts (>67%) were modified by $m^5C$ modification in *Tet2*-deficient AML cells (Figure S7R). Those overlapped transcripts are mainly enriched in the signal pathways related to metabolism, intracellular transport, and purine nucleotide binding (Figure S7S). Taken together, our results suggest that *Tet2* deficiency leads to the accumulation of $m^5C$ in *Tspan13* mRNA, and Ybx1 recognizes $m^5C$ modification, stabilizes *Tspan13* transcript, and increases its overall expression, which in turn leads to the activation of the CXCR4/CXCL12 axis in BM microenvironment (Figure 7P).

## Discussion

Loss-of-function mutations of TET2 are common across a range of blood malignancies (including AML) and confer resistance to standard therapeutics. In the present study, we found that besides loss-of-function mutations in TET2, transcriptional suppression of *TET2* is also common in AML patients, and its decreased expression is associated with shorter overall survival in AML patients. Interestingly, in addition to its canonical role in DNA demethylation, TET2 also functions as an RNA demethylase to post-transcriptionally regulate expression of its mRNA targets such as *Tspan13*. We revealed a previously unappreciated role of TET2-mediated mRNA $m^5C$ demethylation in AML and uncovered the essential biological function of the TET2/$m^5C$/TSPAN13/CXCR4/CXCL12 axis in LSC homing into the BM niche, resulting in the rapid and aggressive leukemogenesis upon *TET2* deficiency. Overall, our study provides novel insight into the cellular/molecular

mechanisms underlying leukemogenesis, LSC homing, and self-renewal, and highlights the therapeutic potential of reactivation of TET2 signaling in treating leukemia patients with *TET2* mutations or transcriptional suppression.

## TET2 in RNA demethylation: beyond the canonical transcriptional gene regulation

Most recently, covalent chemical modifications in RNAs, especially mRNA, are progressively being appreciated as key regulators of RNA metabolism, including stability, translation efficiency, alternative splicing, and nuclear export [3,56]. Albeit over 170 decorations have been detected in RNAs [57], the biological roles of most epitranscriptomic modifications have not been fully defined. The mammalian TET proteins, TET1, TET2, and TET3, are originally discovered as dioxygenases catalyzing DNA demethylation and mainly affect gene expression at the transcriptional level [8–10]. More recently, TET2 has been reported as an RNA-binding protein [58] *in vitro* and *in vivo*, and can oxidize $m^5C$ in abundant non-coding RNAs, such as tRNA, in mouse embryonic stem cells (mESCs) as well as mRNA during myelopoiesis [17,59,60]. In tRNA, both $m^5C$ and its oxidation product $hm^5C$ have been characterized and account for 10% and 0.02% of cytidine, respectively [60]. However current studies reporting the abundance of $m^5C$ and especially $hm^5C$ in mRNA are somehow controversial. Specifically, Guallar et al. [18] and Lan et al. [20] have clarified hundreds of $hm^5C$-modified mRNA transcripts, including the transcripts related to pluripotency, in ESC cells via an antibody-dependent approach. Moreover, they have observed that $hm^5C$ decoration is enriched in chromatin-associated and nascent pre-mRNA, suggesting a co-transcriptional mechanism of mRNA $m^5C$ modification. In contrast, Legrand et al. [54] failed to detect any evidence for the occurrence of $hm^5C$ (the potential oxidated product of $m^5C$) in mRNA in mESCs through LC-MS/MS analysis, which agrees with another independent study [19].

In our study, we have accurately and unbiasedly assessed the abundance of both $m^5C$ and $hm^5C$ modifications in mRNA via *in vitro* (cell-free system) and *in cellulo* strategies. *TET2* deficiency leads to the transcriptome-wide accumulation of $m^5C$ residues, and the opposite is true when TET2 is overexpressed in either primary AML cells or cell lines. According to our results, $m^5C$ accounts for 0.02–0.05% of cytosines in mRNA. Though $m^5C$ abundance is lower than the most prevalent $m^6A$ modification (which usually accounts for 0.2–0.5% of adenosines) in mRNA, it is still much more abundant than other sparse decorations, such as internal $N^7$-methylguanosine ($m^7G$), $N^1$-methyladenosine ($m^1A$), and $N^6$,2′-O-dimethyladenosine ($m^6A_m$) [61–63]. We believe the dynamic and reversible $m^5C$ modification offers the potential of regulating mRNA fate post-transcriptionally. More systemic and comprehensive studies are warranted to dissect the landscape, biological functions, and mechanisms of $m^5C$ in mRNA. In line with the reported studies [19,54], we could not detect the existence of $hm^5C$ modification in mRNA in AML cells either. The possible reasons could be (1) the $hm^5C$ modification in mRNA represents a signal which immediately induces degradation; (2) the $hm^5C$ itself is an unstable oxidation product or occurs transiently during TET2-mediated demethylation of $m^5C$ modification; and/or (3) the abundance of $hm^5C$ modification in mRNA is below the minimum detection limit of QQQ-MS.

Although $m^5C$ is more abundant relative to other rare chemical decorations in mRNA, the $m^5C$-modified mRNA targets of TET2 are still poorly understood. Here we identified *TSPAN13* as a functionally essential and $m^5C$-dependent mRNA target of TET2 and elucidated its pathological role in LSC homing into the BM niche. *TET2* deficiency-induced accumulation of $m^5C$ modification in *TSPAN13* mRNA can be recognized by YBX1, which in turn stabilizes the transcript and increases its overall expression. Genetic depletion of *TSPAN13* can substantially reverse *TET2* deficiency-enhanced LSC homing and self-renewal, which underscores the importance of TET2 activity for mRNA metabolism and post-transcriptional regulation in AML. The $m^5C$ residue in mRNA is mediated by the DNMT2 and NSUN methyltransferase family in the nuclei [21]. However, it's still elusive whether the deposition of $m^5C$ modification in mRNA is co-transcriptionally, and whether there is any link or crosstalk between TET2-mediated epigenetic and epitranscriptomic regulation.

## Targeting leukemic microenvironment to treat TET2-deficient leukemia

Despite improvements in diagnosis and treatment-adapted regimens, the survival rate of AML is still dismal [64]. A combination of cytarabine and anthracycline (e.g., daunorubicin) is the backbone of AML therapy and such approach has not substantially changed over the decades [65]. AML patients with *TET2*-deficiency are poorly responsive to those standard chemotherapy agents. In addition, the antiproliferative therapy is not sufficient to effectively treat leukemias with *TET2* deficiency. Consequently, AML patients with *TET2* deficiency are associated with shorter survival compared to those without TET2 deficiency.

Using various primary AML models, here we showed that *Tet2* deficiency-induced rapid leukemogenesis is not simply attributed to cell proliferation benefits, but largely due to the increased LSC homing and self-renewal. We also found that existence of stromal cells could substantially enhance the colony-forming ability of TET2-deficient AMLs. Such phenotype might be attributed to the soluble factors, such as SCF, CXCL12, and ANGPT, which are secreted at high levels by BM stromal cells [66]. The direct interplays between the leukemia cells and BM stromal cells have been postulated to be essential for chemoresistance and relapse of leukemia [67]. The existence of BM stromal cells protected AML cells from chemotherapy drugs-induced cell killing and leads to drug resistance. The CXCR4/CXCL12 axis plays a central role in trafficking LSCs into the BM niche. *TET2* deficiency in AML promotes the TSPAN13/CXCR4 axis via an mRNA $m^5C$-dependent manner, and thereby enhances LSCs homing and self-renewal. Several small molecule compounds targeting CXCR4 have been developed [32,68]. Pharmacological inhibition of CXCR4 induced the mobilization of AML blast cells into circulation, sensitized AML to chemotherapy, and extensively elongated the survival in the treated mice, demonstrating the pivotal role of the CXCR4/CXCL12 axis in the pathogenesis of AML and drug resistance. It would be interesting to test whether restoration of TET2 activity can block the homing of LSCs into BM niche via silencing the TSPAN13/CXCR4 signaling, whether "priming" leukemia cells with TET2 activator agent can render them more sensitive to standard chemotherapeutic drugs and targeted therapy agents such as CXCR4 inhibitors.

Collectively, our findings suggest that targeting the leukemic microenvironment to disrupt the interaction between leukemia cells and stromal cells could be a promising therapeutic strategy to treat TET2-deficient AMLs, and such a therapeutic strategy could be extended to other cancer types with TET2 mutation and/or suppression.

### Limitation of the study

In the present study, we utilized mRNA bisulfite sequencing to identify $m^5C$ sites. However, the harsh bisulfite treatment may lead to random degradation of mRNAs. Furthermore, mRNA bisulfite sequencing is unable to distinguish $m^5C$, $hm^5C$, and $m^4C$. Therefore, the development of more accurate methods for $m^5C$ sequencing is necessary to gain a better understanding of the role of $m^5C$ modification in mRNA metabolism. Considering that the CXCR4-CXCL12 signaling plays a pivotal role in mediating AML cell homing in the BM microenvironment, it is important to systematically investigate whether and how TET2 deficiency in AML blast cells remodels BM microenvironment to facilitate their homing, survival and proliferation/self-renewal. Given that loss of TET2 substantially triggers the activation of the CXCR4 signaling, it is worth assessing the therapeutic potential of CXCR4 inhibitors alone or in combination with other therapeutics for the treatment of TET2-deficient leukemia.

## STAR Methods

### RESOURCE AVAILABILITY

**Lead Contact—**Further information and requests for resources and reagents may be directed to and will be fulfilled by the Lead Contact, Jianjun Chen (jianchen@coh.org).

**Materials Availability—**All cell lines, plasmids, and other stable reagents generated in this manuscript are available from the Lead Contact under a complete Materials Transfer Agreement.

### Data and Code Availability

- The RNA-seq, mRNA half-life profiling, and mRNA Bis-seq data have been deposited at GEO and are publicly available as of the date of publication. Accession numbers are listed in the key resources table.
- This paper does not report any original code.
- Any additional information required to reanalyze the data reported in this work paper is available from the Lead Contact upon request.

### EXPERIMENT MODEL AND SUBJECT DETAILS

**Primary AML Patient and Healthy Donor Specimens—**Human AML patient samples were obtained at the time of diagnosis, after treatment, or relapsed with informed consent at City of Hope Hospital, Cincinnati Children's Hospital, or Dana-Farber/Harvard Cancer Center, in congruence with the approved protocol by the institutional review board (IRB). The characteristics of AML patients are detailed in Table S1. The samples from healthy donors were collected from the Healthy Donor Center in Cincinnati Children's

Hospital under the institute's approved IRB protocol. Erythrocytes lysis was performed on the samples, and the mononuclear cells (MNCs) were cryopreserved at −150°C for further study.

**Cell Culture—**All cell lines were obtained from the sources listed in the key resources table. HEK293T and C1498 were cultured in endotoxin-free DMEM medium (Life Technologies) supplemented with 10% fetal bovine serum (FBS) (100–106, Gemini Bio-Products), 1% penicillin/streptomycin (15–140-122, Thermo Fisher Scientific), and 2.5 μg/mL Plasmocin prophylactic (ant-mpp, InvivoGene); Mono Mac 6 was maintained in RPMI 1640 supplemented with 10% FBS plus 2 mM L-glutamine (25030–081, Thermo Fisher Scientific), 1× non-essential amino acids (11140050, Gibco), 1 mM sodium pyruvate (11360070, Thermo Fisher Scientific), 10 mg/ml human insulin (12585014, Thermo Fisher Scientific); OP9 cells were cultured in alpha-MEM (32571101, Thermo Fisher Scientific) supplemented with 20% FBS plus 2.2 g/L sodium bicarbonate. All the cell lines were routinely tested for mycoplasma contamination using a PCR Mycoplasma Detection Kit (G238, Applied Biological Materials).

**Animals—**All congenic recipient mice were NCI C57 B6.SJL ($CD45.1^{+}$, RRID: IMSR_CRL:564) purchased from Charles River Laboratories (Wilmington, MA). The immune-incompetent NOD.Cg-$Rag1^{tm1Mom}$ $Il2rg^{tm1Wjl}$ Tg (CMV-IL3, CSF2, KITLG) 1Eav/J (NRGS, RRID: IMSR_JAX:024099) mice were originally purchased from the Jackson Laboratory and bred under pathogen-free conditions. All animal experiments were done in accordance with the guidelines of the institutional guidelines and Institutional Animal Care and Use Committee (IACUC) protocols approved by City of Hope. All these mice were maintained on a 12-hour:12-hour, light: dark cycle with food and water *ad libitum*. For each experiment, 6- to 8-week-old mice were randomly allocated to experimental groups.

## METHOD DETAILS

**Plasmid Construction—**The catalytic domain of TET2 (pcDNA3-TET2-CD) kindly provided by Dr. Yue Xiong, the full-length Tet2 (pcDNA3–1xFlag-Tet2) (60939, Addgene), Flt3-ITD (pMSCV-Flt3-ITD-Y591F/Y919F) (74499, Addgene), and murine cDNA made from MA9 leukemic cells were served as templates to generate 3×FLAG-tagged TET2 CD, Tet2 CD, Flt3-ITD, Tspan13, and Ybx1 fragments by PCR amplification with CloneAmp™ HiFi PCR Premix (639298, Takara Bio). The PCR fragment of TET2 CD was ligated into pCDH empty vector and the rest of fragments were ligated to the MSCV vector with In-Fusion HD Cloning Plus Kits according to the manufacturer's instruction (638909, Takara Bio). shRNAs targeting *Tspan13* and *Ybx1* were generated as previously described with mild revision [79].The palindromic DNA oligo was annealed by gradient cooling to form a double-strand oligo and then ligated to the pLKO.1-puro vector cleaved by AgeI and EcoRI restriction enzymes with T4 DNA ligase at 16°C for 2 hours or overnight. All the primers used for molecular cloning were listed in Table S2. The plasmids were extracted using QIAprep Spin Miniprep Kit (27104, Qiagen) and then verified by Sanger sequencing (Eton Bioscience).

**Lentivirus and Retrovirus Preparation and Infection—**These assays were conducted as previously described with minor modifications [2,80]. All lentivirus particles for overexpression and knockdown plasmids were packaged using the 2nd-generation package system. Briefly, 2.25 μg psPAX2, 0.75 μg pMD2.G), and 3 μg target plasmids diluted in Opti-MEM medium (31985070, Thermo Fisher Scientific) were incubated with X-tremeGENE™ HP DNA Transfection Reagent (6366546001, Sigma-Aldrich). For retrovirus packaging, 1.5 μg plasmids in MSCV backbone and 1.5 μg pCL-ECO vector ((IMGENEX, San Diego, CA) incubated with DNA transfection reagent. The DNA mixture were then co-transfected into HEK293T cells in 6-cm cell culture dishes. The following morning, medium was replaced with 4 mL DMEM complete medium. The virus-containing supernatant were harvested at 48 h and 72 h post-transfection and filtered through a 0.45μm syringe filter or centrifuged for 15 min at 3000g at 4°C. The viral supernatant was added to cells in the presence of 4–8 μg/mL polybrene (H9268, Sigma-Aldrich). To infect the suspension cells, cells were subjected to two rounds of spinoculation at 32°C for 2h. The infected cells were selected with 2 μg/mL puromycin (for pCDH, MSCV-PIG and pLKO.1 backbone) or 1 mg/mL G418 (MSCV-neo backbone) (10131–02, Life Technologies) after 48-hour infection.

**Cell Viability and Proliferation Assay—**Cell viability and proliferation were determined with Cell Counting Kit 8 (CK04, Dojindo). The cells were seeded into 96-well plates at a density of $1 \times 10^4$ cells per well at a final volume of 100 μl. Per the manufacturer's instruction, 10 μl dye solution was added into the well at indicated time point. After incubation at 37°C for 2–3 hours, the absorbance at 450 nm was determined using BioTek Gen5 system (BioTeck, USA).

**Cell Cycle Assay—**The percentage of cells located at G0/G1, S, and G2/M phases was assessed by Propidium Iodide (PI, P4170, Sigma-Aldrich) DNA staining. $1 \times 10^6$ cells were harvested, washed with PBS once, resuspended in 1 ml Krishan's buffer supplemented with 0.05 mg/ml PI, 0.02 mg/ml ribonuclease A, 0.1% trisodium citrate, and 0.3% NP-40, and incubated at 37°C for 30 minutes. The samples were then applied to flow cytometry analysis directly.

**Flow Cytometry Analysis—**Flow cytometry analysis of stem cell and differentiation markers was performed as described previously [81]. The mouse samples collected from peripheral blood, bone marrow, and spleen were depleted red blood cells with ammonium chloride solution (07850, STEMCELL Technologies) before staining. Cells were washed with PBS, re-suspended in ice-cold FACS buffer supplemented with anti–mouse CD16/32 (14–0161-82, eBioscience) to block non-specific binding and desired antibodies at 4°C for 30min at dark and mix every 10 minutes. Then cells were washed with PBS and resuspended in IC Fixation Buffer (eBioscience). The samples were analyzed on BD FACS FortessaX-20 (BD Biosciences, USA) and the results were analyzed with FlowJo V10 Software.

The following antibodies were used for flow cytometry: CD45.2-FITC (109806, Biolend), anti-lineage markers-eFluor 450 (88–7772-72, eBioscience), c-Kit-APC (17–1171-83, eBioscience), c-Kit-APC-Cy7 (135136, BioLegend), Sca-1-PE (12–5981-82, eBioscience), Mac-1-PerCP-Cyanine5.5 (45–0112-82, eBioscience), Gr-1-PE (12–5931-81, eBioscience), 7-AAD (559925, BD Bioscience), CD34-APC (128612, Biolend), CD16/CD32-PE-Cy7

(25–0161-82, Thermo Fisher Scientific), CD8 (17–0083-81, eBioscience), CD45-APC (17–9459-42, Thermo Fisher Scientific), CD33-PE (12–0339-42, Thermo Fisher Scientific), CXCR4 (phospho Ser339) (BS-12256R, Thermo Fisher Scientific), and CXCR4-PE (146505, BioLegend).

**EdU Proliferation Assay—**The EdU proliferation staining was performed following the manufacturer's recommendation using the EdU Staining Proliferation Kit (ab219801, Abcam). $2 \times 10^6$ cells were seeded into a 6-well plate and incubated with 20 μM EdU at 37°C for 2 hours. The cells were then harvested, washed, and fixed with fixative solution for 15 min. Then the cells were washed and permeabilized for 15 min. Finally, washed cells were incubated with reaction mix to fluorescently label EdU for 30 min at room temperature protected from dark, washed, and re-suspended in FACS buffer for further analysis.

***In Vitro* Colony-Forming and Replating Assay—**The serial colony-forming assay was employed as described previously with minor modifications [82]. Mouse BM progenitor cells ($Lin^-$ or $c\text{-}Kit^+$) were enriched from 6- to 8-week-old C57BL/6J ($CD45.2^+$) mice upon 150 mg/kg 5-fluorouracil (5-FU) treatment for 5 days with Lineage Cell Depletion Kit (130–090-858, Miltenyi Biotec) or CD117 MicroBeads (130–091-224, Miltenyi Biotec) and infected with MSCV-based retroviruses as before mentioned. The transduced cells were seed at a density of $1 \times 10^4$ per 35 mm culture dishes (27150, STEMCELL Technologies) in ColonyGEL (1201, ReachBio Research Labs) in the presence of 10 ng/ml of murine recombinant IL-3, IL-6, GM-CSF, and 50 ng/ml of murine recombinant SCF, using G418 and/or puromycin as selectable markers. The colonies were incubated at 37°C in a humidified atmosphere with 5% $CO_2$ in air for 6 to 7 days. Serial replating was then conducted by collecting and replating colony cells every 7 days. Colony numbers were enumerated and compared for each passage.

**Syngeneic Bone Marrow Transplantation (BMT)—**For primary BMT, transformed cells ($5 \times 10^5$) were mixed with $1 \times 10^6$ $CD45.1^+$ BM 'helper' cells and transplanted into lethally irradiated 6- to 8-week-old NCI C57 B6.SJL ($CD45.1^+$) recipient mice. For secondary BMT, leukemia cells sorted from bone marrow of primary leukemia mice were injected into sub-lethally irradiated recipient mice. $1–5 \times 10^5$ $CD45.2^+$ leukemic cells isolated from the BM of primary recipients were transplanted into $CD45.1^+$ recipient mice with or without sub-lethally irradiated.

**AML PDX Model and 'Human-in-Mouse' Xenograft Model—**Both female and male NRGS mice were used as hosts for xenotransplantation experiments. For each experiment, both female and male mice were randomly assigned to each group. In the "Human-in-Mouse" model, Mono Mac 6 ($1 \times 10^5$) cells with or without human TET2 CD overexpression were re-suspended in PBS and intravenously transplanted into NRGS recipient mice. We also utilized AML PDX cell [83], #2017–129, to further perform xenotransplantation. $2 \times 10^5$ #2017–129 cells were implanted into NRGS mice, and AML progression was monitored using *in vivo* bioluminescence imaging. To assess AML burden, mice were euthanized at the same time and stained with anti-CD45 (17–9459-42, Fisher

Scientific) and anti-CD33 (12–0339-42, Thermo Fisher Scientific) antibodies and subjected to flow cytometry.

***In Vitro* Co-Culture Assay and Migration Assay—**These assays were performed as described previously with minor modifications [84]. Briefly, $1.5 \times 10^4$ OP9 cells were seeded in the lower chamber in 600μl culture medium overnight. Then, a total number of $2 \times 10^5$ murine AML cells (*Tet2*$^{+/+}$ or *Tet2*$^{-/-}$) were washed with serum-free PBS once, resuspended in the culture medium and seeded in the upper chambers of Transwell (3 μm, 3415, Corning). After 12–24 hours of incubation, migrated AML cells in the lower chambers were harvested and counted.

**Limiting Dilution Assays (LDAs)—**LDAs were conducted as previously described [82]. For *in vitro* LDAs, the murine NRAS/AE9a, NRAS/PML-RARA, or MA9 AML cells were suspended in ColonyGEL medium supplied with murine 50 ng/ml SCF, 10 ng/ml IL-3 and IL-6, 1 mg/mL G418, and 2 μg/mL puromycin and plated in 48- or 96-well plates with 6–8 different doses of cell number for each group. The number of wells containing spherical colonies was counted after 5–7 days. For *in vivo* LDA, MA9 AML cells with or without *Tet2* knockout were injected into non-irradiated 6- to 8-week-old CD45.1$^+$ recipient mice with six doses of cells for each group. The number of recipient mice that developed full-blown leukemia within 80 days post-transplantation was counted in each group with each dose of cells. The frequency of LSCs was determined by the ELDA online tool: http://bioinf.wehi.edu.au/software/elda/ [85].

**Histopathology Analysis—**Livers and spleens were dissected from mice and fixed with formalin overnight. Paraffin embedding and H&E staining were conducted by the Pathology Core at City of Hope. PB and BM smears were briefly fixed in methanol for 30 seconds, followed by two-minute incubation with Wright-Giemsa Stain (24985, Polysciences), 6-minute incubation with Wright-Giemsa Stain/Buffer (24984, Polysciences) mixture, and a 2-minute rinse in Wright-Giemsa Buffer. All the slides were examined with Widefield Zeiss Observer 7 microscope.

***In vivo* Bioluminescence Imaging—***In vivo* bioluminescence imaging was conducted to monitor *in vivo* engraftment of AML cells in recipient mice. The mice were weighed, injected intraperitoneally with 150 mg/kg BW D-luciferin (LUCK-2G, Goldbio) in PBS solution, and then anesthetized with isoflurane. Ten minutes after injection, the mice were imaged with Lago X (Spectral Instruments Imaging). The bioluminescent signals were quantified using Aura imaging software (Spectral Instruments Imaging). Total flux values were determined and presented in photons/second/cm$^2$/steradian.

***In vivo* Homing Assay—**Homing assays were performed as previously described [86]. Briefly, a total number of $5–10 \times 10^6$ AML cells were labeled with 5(6)-carboxy fluorescein diacetate succinimidyl ester (CFSE) (65–0850-84, eBioscience) or stably expressed GFP and transplanted into the lethally irradiated CD45.1$^+$ recipient mice or NRGS mice. Homing of the AML cells in the BM were measured at 16 h or at indicated timepoint after transplantation by flow cytometric analysis and confocal imaging. For the AMD 3100

inhibition group, MA9 *Tet2*$^{-/-}$ cells were treated with 0.1mg/ml AMD 3100 for 20 hours before being labeled by CFSE.

**Immunofluorescent Staining of Long Bones—**Long bones (femurs or tibias) from the mice were processed, sectioned, and imaged as described previously [87]. Briefly, the fresh long bones were dissected from the leukemic mice and immediately fixed with 4% paraformaldehyde for 4 hours. The fixed bones were then decalcified in 0.5M EDTA (pH 7.4–7.6) for 24 to 48 hours and then incubated in ice-old cryoprotectant (CPT) solution at 4°C for 24 hours. The decalcified long bones were then embedded in tissue molds with embedding media (EBM). After drying at room temperature and stored at −80°C overnight, the bones were sectioned longitudinally using a microtome with a thickness of 40 μm. The sections were rehydrated, permeabilized, blocked, and incubated with PE-conjugated osteopontin (OPN) (IC808P, R&D Systems) overnight at 4°C. After washing, the slides were mounted with DAPI mounting medium to stain the nuclei. Imaging was performed using a confocal microscope (Zeiss, LSM880) and analyzed using the Zen program (Zeiss).

**RNA Extraction and Real-Time Quantitative PCR (RT-qPCR) Analysis—**Total RNA samples were extracted from cells using TRIzol reagent according to the manufacturer's instructions. Reverse transcriptase reaction was performed with 200–1000 ng of total RNA or immunoprecipitated RNA samples in 10 μL reaction volume using the QuantiTect Reverse Transcription kit (205314, QIAGEN) following the manufacturer's instructions. Quantitative PCR (qPCR) was then performed with Maxima SYBR Green qPCR Master Mix (2×) (FEPK0253, Thermo Fisher) on the QuantStudio 7 Flex PCR system (Thermo Fisher Scientific). GAPDH, ACTIN, and/or 18S rRNA were used as endogenous control and each reaction was run in triplicates. All the primers are listed in Table S2.

***In vitro* (cell-free) Demethylation Assay with TET2 Protein—**To assess the enzymatic activity of TET2 on DNA and RNA, the synthesized 30-mer single-stranded RNA (ssRNA) with internal $m^5C$ modification (5'-CAG UAA CUG UGG UC($m^5C$) GGU AAC UGA CUU GCA-3') (Dharmacon), or a single-stranded DNA (ssDNA) with a single 5mC situated in the same sequence context (Integrated DNA Technologies), or *in vitro* transcribed $m^5C$-bearing *TSPAN13* were served as substrates. Briefly, 2.5 μM RNA/DNA oligos or 250 ng *TSPAN13* mRNA were incubated with 0.25 μg catalytic domain of TET2 protein (31418, Active Motif) in 50 μL reaction buffer containing 50 mM HEPES, pH 8.0, 100 μM NaCl, 75 μM $Fe(NH_4)_2(SO_4)_2$, 1 mM 1,4-Dithiothreitol (DTT), 2 mM L-ascorbate, 100 μM alpha-ketoglutarate, and 100 μM ATP at 37°C for 20–120 minutes. The RNA or DNA were purified using Oligo Clean & Concentrator kit (D4061, Zymo Research). The activity was detected by dot blot or QQQ-MS.

***In vitro* Transcription—**The *TSPAN13* mRNA was obtained from *in vitro* transcription by using MEGAscript T7 kit (AM1333, Invitrogen). Briefly, cDNAs were synthesized with total RNA extracted using SuperScript III First-Strand Synthesis System (18080051, Invitrogen). Then the *TSPAN13* was amplified by PCR which contains a T7 promoter sequence at its 5′ terminus using Platinum SuperFi II DNA Polymerase (12361010, Thermo Scientific). Primers employed to generate DNA templates are listed in Table S2. Purified

*TSPAN13* DNA was subjected to an *in vitro* transcription reaction with MEGAscript T7 RNA polymerase (AM1354, Thermo Fisher Scientific) at 37 °C for 4 h in a 50 μL reaction mixture containing 5-methylcytidine-5'-triphosphate (5mCTP) (N-1014–1, TriLink Biotechnologies), according to the manufacturer's instructions. DNA template was digested with TURBO DNase (AM2239, Thermo Fisher Scientific). Transcripts were then purified by MEGAclear Transcription Clean-Up Kit (AM1908, Thermo Fisher Scientific).

**UHPLC-QQQ-MS/MS—**The levels of $m^5C$, $hm^5C$, 5mC, and 5hmC measured by ultra-high-performance liquid chromatography coupled with triple-quadrupole tandem mass spectrometry (UHPLC-QQQ-MS/MS). The nucleic acids were digested in one-step procedure as previously described [88]. 200 ng-1000 ng DNA or RNA samples were digested with 50 μL digestion mix containing 2.5 U Benzonase (E1014, Sigma-Aldrich), 3 mU phosphdiesterase I (P3243, Sigma-Aldrich), 2 U alkaline phosphatase (EF0651, Thermo Fisher Scientific), 20 mM Tris-HCl, pH7.9, 100 mM NaCl, and 20 mM $MgCl_2$ at 37°C for 6 hours. The digestion mixture was diluted to 200 μl by LC-MS grade water and analyzed by Agilent 6410 Triple Quadrupole Tandem Mass Spectrometer with an Agilent 1290 HPLC. Nucleosides were separated by the Agilent RRHD SB-C18 column (2.1 × 50mm,1.8μm,1200 bar). 0.1% formic acid (FA) in ddH2O as Solvent A and 0.1% FA in acetonitrile as Solvent B were employed as the mobile phase. The amounts of nucleosides were calibrated by standard curves obtained from pure nucleoside standards (Cayman Chemical Company).

**Dot Blot Assay—**Dot blot assays for quantification of 5mC and 5hmC in DNA and $m^5C$ and $5hm^5C$ in RNA were conducted as previously reported [17,63]. Genomic DNA was isolated with a DNeasy Blood and Tissue Kit (69506, QIAGEN) according to the manufacturer's instructions. DNA was denatured in 0.1 N NaOH at 99°C for 5 minutes and neutralized with 0.66 M ammonium acetate. RNA was denatured in RNA incubation buffer (65.7% formamide, 7.77% formaldehyde, and 1.33× MOPS) at 65 °C for 5 min, chilled on ice immediately, and mixed with equal volume of 20 × standard saline citrate (SSC) buffer. The denatured samples were spotted onto an Amersham Hybond-$N^+$ membrane (45–000-927, GE Healthcare) using an assembled Bio-Dot apparatus (Bio-Rad) and followed by UV-crosslink (254 nm UV for 5 min). Then the membrane was stained with 0.02% methylene blue in 0.3 M sodium acetate (pH 5.2), blocked with 5% non-fat milk in 1×PBST for 1 h, and incubated with anti-5mC antibody (1:5000, 39649, Active Motif) or anti-5hmC antibody (1:5000, 39769, Active Motif) overnight at 4 °C. Then the membrane was washed for three times with 1×PBST, incubated with HRP-conjugated secondary antibody (1:5000) for 1h at room temperature. Dot blot was developed with Amersham ECL Prime Western Blotting Detection Reagent (45–010-090, GE Healthcare) and captured by a chemiluminescent imaging system.

**Gene-specific $m^5C$ RNA Immunoprecipitation and qPCR—**$Poly(A)^+$ RNA was enriched from total RNA with polyATract mRNA isolation system IV kit (Z5310, Promega) following manufacturer's instructions. $m^5C$ RNA immunoprecipitation (MeRIP) was performed as described previously with some modifications [55]. 11 μg mRNA was fragmented into 100–200 nt in length using NEBNext® Magnesium RNA Fragmentation

Module (E6150S, New England Biolabs). The fragmented RNA was purified and 5 μg mRNA was incubated with 5 μg anti-$m^5C$ antibody (ab10805, Abcam) or mouse IgG (NI03, Millipore) in 400 μL 1× IP buffer (150 mM NaCl, 0.1% NP-40, 10 mM Tris-HCl, pH 7.4, 0.4 U/ml RNase inhibitor) at 4°C overnight and one-tenth of fragmented RNA was saved as input control. Then the mRNA was incubated with washed conjugated Protein A/G Magnetic Beads (88803, Thermo Fisher Scientific) at 4°C for three hours. The magnetic beads were then washed four times with 1× IPP buffer and the bound RNAs were recovered by proteinase K digestion. The IP RNA fragments were finally eluted in using RNA Clean & Concentrator (R1015, Zymo Research). Input RNA and MeRIP-ed RNA were further analyzed by qPCR. Cycle threshold (Ct) values (ΔΔCt method) were used to determine the relative enrichment of $m^5C$ in each sample.

**Nuclear Run-on Assay—**Nuclear run-on assay was conducted as previously described [63]. Nuclei were isolated from WT and *Tet2*-null cells with Nonidet P-40 lysis buffer (10 mM Tris-Cl, pH 7.4, 10 mM NaCl, 3 mM $MgCl_2$, and 0.5% NP-40). The enriched nuclei were suspended in 396 μL nuclear freezing buffer (50 mM Tris-Cl, pH 8.3, 40% glycerol, 5 mM $MgCl_2$, and 0.1 mM EDTA). Then 100 μL of 5× run-on buffer (25 mM Tris-Cl, pH 8.0, 750 mM KCl, 12.5 mM $MgCl_2$, 1.25 mM each of ATP, GTP, and CTP) was added into the nuclei along with 4 mL biotin-16-UTP (11388908910, Sigma-Aldrich) to initiate the nuclear run-on reaction. After incubation at 29°C for 30 min, the reaction was quenched by adding 0.75 μL 1M $CaCl_2$, and 3 μL RNase-free DNase I and incubating for 10 min at 29°C. RNA was recovered with the RNeasy mini kit (74104, QIAGEN) and eluted in 50 μL of nuclease-free water. One-tenth of RNA was saved as ‘‘total nuclear RNA’’. Dynabeads M-280 streptavidin (11205D, Thermo Fisher Scientific) resuspended in binding buffer (10 mM Tris-HCl, pH 7.5, 1 mM EDTA and 2 M NaCl) were mixed with an equal volume of the RNA samples and incubated firstly at 42°C for 20 min and then room temperature for 2 hours. After washing with 2× SSC, the beads were resuspended in 25 μL of nuclease-free water and subjected to qPCR analysis. The qPCR products were then applied on a 2% agarose gel analysis and captured by Gel DocTM XR System (BIO-RAD).

**Protein Extraction and Western Blot Assay—**For total protein extraction, washed cell pellets were lysed in RIPA buffer (R0278, Sigma-Aldrich) supplemented with 5mM EDTA, 1 × Halt phosphatase inhibitor cocktail (78420, Thermo Fisher Scientific), and 1 × Halt protease inhibitor cocktail (78429, Thermo Fisher Scientific) on ice for 20 minutes, sonicated, and centrifuged at 20,000 g at 4°C for 15 minutes. Protein concentration was quantified with Bio-Rad Protein Assay Dye Reagent Concentrate (5000006, Bio-Rad) and bovine serum albumin (Protein Standard II #5000007, Bio-Rad). Protein lysates were diluted with 4× Laemmli Sample Buffer (5000007, Bio-Rad) containing β-mercaptoethanol and denatured at 95°C for 10 min.

Western blot was conducted as previously described [63,82]. Briefly, equal amounts of protein extracts (20–50 μg) were separated by 6%−10% SDS-PAGE gels and onto polyvinylidene difluoride (PVDF) membranes. The blots were blocked with 5% non-fat milk in PBST and incubated with diluted primary antibodies in 1% (w/v) BSA in PBST overnight at 4°C. Then membranes were washed with 1 × PBST, incubated with secondary antibody, and

detected by Pierce ECL Western Blotting Substrate (PI32106, Thermo Fisher Scientific) or GE Healthcare Amersham ECL Prime Western Blotting Detection Reagent (45010090, GE Healthcare). The following primary antibodies were used for Western blotting: anti-GAPDH (1:5000, 10494–1-AP, Proteintech), anti-Vinculin (1:5000, sc-25336, Santa Cruz Biotechnology), anti-FLAG (1:3000, F3165, Sigma-Aldrich), anti-CXCR4 (1:2000, 60042–1-IG, Proteintech), anti-CXCR4 (phospho Ser339) (1:2000, GTX32281, GeneTex; 1:1000, BS-12256R, Thermo Fisher Scientific), anti-TSPAN13 (1:500, abx214152, Abbexa), anti-Lamin A/C (1:2000, 4777, Cell Signaling Technology), and anti-α-Tubulin (1:5000, 3873S, Cell Signaling Technology). Secondary antibodies used in this study include Horseradish peroxidase (HRP) conjugated Goat Anti-Mouse IgG H&L (HRP) (ab6789, abcam) and Goat Anti-Rabbit IgG H&L (HRP) (ab6721, abcam).

**RNA Stability Assay—**The cells were treated with 5 μg/ml actinomycin D (A9415, Sigma-Aldrich) for indicated time to assess RNA stability of *TSPAN13* transcript. Total RNA was extracted from cells using TRIzol reagent for RT-qPCR analysis. The turnover rate and half-time of mRNA were estimated according to previously described [63,82]. Since the actinomycin D closes mRNA transcription, the half-life of mRNA concentration at a given time ($dC/dt$) is proportional to both the rate constant of mRNA decay ($k_{decay}$) and mRNA concentration ($C$) as shown in the following equation:

$$dC/dt = -k_{\text{decay}}$$

Thus, the rate constant for mRNA degradation $k_{decay}$ could be estimated by the derivation of the equation:

$$\text{In}(C/C0) = -k_{\text{decay}} \cdot t$$

$C_0$ is the concentration of mRNA at time 0, $t$ is the transcription inhibition time, and $C$ is the mRNA concentration at the time t. To calculate the half-time ($t_{1/2}$) of RNA, which means $C/C_0 = 50\%/100\% = 1/2$, the equation can be rearranged into the following equation:

$$\text{In}(1/2) = -k_{\text{decay}} \cdot t_{1/2}$$

from where:

$$t_{1/2} = ln2/k_{\text{decay}}$$

**mRNA Half-time Profiling and Data Analysis—**WT and *Tet2*-null *NRAS/AE9a* AML cells were treated with 5 μg/ml actinomycin D (A9415, Sigma-Aldrich) for 0, 4, and 8 hours. At each time point, cells were rapidly harvested, and total RNA was extracted using TRIzol reagent. The RNA samples were subsequently subjected to sequencing on Illumina NovaSeq 6000 system with a paired-end 150-base pair (bp) read length. Reads were mapped to mm10 genome by STAR [76]. Gene expression (RPKM) was calculated by RSEM. The degradation

rate and half-life of RNA were calculated using the formula mentioned earlier. The average values of the half-lives were calculated as described previously[89].

**mRNA Bisulfite-seq and Data Analysis—**Total RNA extraction from WT and *Tet2*-null *NRAS/AE9a* AML cells was performed using TRIzol reagent (15596–018, Thermo Fisher Scientific) and then was enriched for poly(A) RNA using polyATract mRNA isolation system IV kit (Z5310, Promega) following manufacturer's instructions with the following modifications. The purified RNA was then subjected to bisulfite treatment using EZ RNA Methylation Kit (R5002, Zymo Research). Briefly, 1μg mRNA per sample in 20 μL nuclease-free water was mixed with 130 μl of RNA Conversion Reagent in a PCR tube. Then the mixture was incubated in a thermal cycler following 70°C for 10 minutes and 54°C for 50 minutes to convert unmethylated cytosine residues to uracil. The converted RNA was then subjected to column-based purification and next-generation sequencing using Illumina HiSeq 2500 platform with 70 million single-end reads per replicate sample. Adaptors were trimmed and low-quality bases were removed by Cutadapt [90]. Clean reads were mapped to the mouse reference genome (mm10) using meRanGh from meRanTK [91]. The $m^5C$ sites were determined using meRanCall, the methylation caller of meRanTK with a false discovery rate < 0.01. Sites with a coverage depth ≥ 30, methylation level ≥ 0.1, and methylated cytosine depth ≥ 5 were considered high-confidence $m^5C$ sites [92].

**RNA-seq and Data Analysis—**For RNA-seq, total RNA extraction from WT and *Tet2*-null *NRAS/AE9a* cells was performed using TRIzol reagent (15596–018, Thermo Fisher Scientific) according to the manufacturer's instructions. Total RNA was subjected to depletion of DNA and rRNA. RNA integrity was assessed by 2100 Bioanalyzer (Agilent Technologies, Santa Clara, USA). RNA library preparation was conducted using KAPA Stranded mRNA-Seq Kit (Illumina Platforms) (Kapa Biosystems, Wilmington, USA) with 10 cycles of PCR amplification and purified by AxyPrep Mag PCR Clean-up kit (Thermo Fisher Scientific). Libraries were run on an Illumina HiSeq 2500 (Illumina, San Diego, CA, USA) instrument in a 51 bp single-end run, generated by the TruSeq SR Cluster Kit V4-cBot-HS (Illumina). Sequencing reads were trimmed for adaptor sequence, masked for low-quality sequence by Cutadapt [90], and aligned to mm10 genome by STAR [76]. Per million mapped reads (RPKM) of each gene were calculated by RSEM [75], and $p < 0.05$ was set as the threshold of the differential expressions. The reads distributed in a specific transcript were displayed by IGV [77]. Gene Set Enrichment Analysis (GSEA) and hallmark gene sets in Molecular Signatures Database (MSigDB) [78] were hired to calculate enriched pathways.

## QUANTIFICATION AND STATISTICAL ANALYSIS

Data were analyzed with GrapPad Prism 9 and were presented as mean ± SEM or mean ± SD as indicated. Statistical Significance was calculated using two-tailed, unpaired Student's t-tests, paired t-test, one-way ANOVA, or two-way ANOVA. Pearson tests were performed for correlation analysis. Kaplan-Meier survival curves were plotted with GraphPad Prism 8 and the *P* values were calculated using the log rank test. $p < 0.05$ was considered a significant difference. For Western blot results, representative figures from three biological replicates were shown.

## Supplementary Material

Refer to Web version on PubMed Central for supplementary material.

## Acknowledgments

We thank for Dr. Gang (Greg) Wang for kindly providing MSCV-DNMT3A$^{R882H}$ and MSCV-DNMT3A$^{R882H}$-NRAS$^{G12D}$. This work was supported in part by the National Institutes of Health (NIH) grants R01 CA214965 (J.C.), R01 CA243386 (J.C.), R01 CA236399 (J.C.), R01 CA271497 (J.C.), R01 DK124116 (J.C.), the Simms/Mann Family Foundation (J.C.), Leukemia Research Foundation New Investigator Research Grant (R.S.), The Margaret E. Early Medical Research Trust (R.S.), AASLD Foundation PNC22-261362 (R.S.), and T32 CA186895 (B.T.). J.C. is a Leukemia & Lymphoma Society (LLS) Scholar. Z.L. is a Research Scholar of American Cancer Society. S.S. is a Scholar of the American Society of Hematology.

## References

1. Huang H, Jiang X, Li Z, Li Y, Song CX, He C, Sun M, Chen P, Gurbuxani S, Wang J, et al. (2013). TET1 plays an essential oncogenic role in MLL-rearranged leukemia. Proc Natl Acad Sci U S A 110, 11994–11999. 10.1073/pnas.1310656110.
2. Li Z, Weng H, Su R, Weng X, Zuo Z, Li C, Huang H, Nachtergaele S, Dong L, Hu C, et al. (2017). FTO Plays an Oncogenic Role in Acute Myeloid Leukemia as a N(6)-Methyladenosine RNA Demethylase. Cancer Cell 31, 127–141. 10.1016/j.ccell.2016.11.017. [PubMed: 28017614]
3. Huang H, Weng H, Deng X, and Chen J. (2020). RNA modifications in cancer: functions, mechanisms, and therapeutic implications. Annual Review of Cancer Biology 4, 221–240.
4. Shih AH, Abdel-Wahab O, Patel JP, and Levine RL (2012). The role of mutations in epigenetic regulators in myeloid malignancies. Nat Rev Cancer 12, 599–612. 10.1038/nrc3343. [PubMed: 22898539]
5. Tefferi A., Lim KH., and Levine R. (2009). Mutation in TET2 in myeloid cancers. N Engl J Med 361, 1117; author reply 1117–1118. 10.1056/NEJMc091348. [PubMed: 19741235]
6. Quivoron C, Couronne L, Della Valle V, Lopez CK, Plo I, Wagner-Ballon O, Do Cruzeiro M, Delhommeau F, Arnulf B, Stern MH, et al. (2011). TET2 inactivation results in pleiotropic hematopoietic abnormalities in mouse and is a recurrent event during human lymphomagenesis. Cancer Cell 20, 25–38. 10.1016/j.ccr.2011.06.003. [PubMed: 21723201]
7. Tefferi A, Pardanani A, Lim KH, Abdel-Wahab O, Lasho TL, Patel J, Gangat N, Finke CM, Schwager S, Mullally A, et al. (2009). TET2 mutations and their clinical correlates in polycythemia vera, essential thrombocythemia and myelofibrosis. Leukemia 23, 905–911. 10.1038/leu.2009.47. [PubMed: 19262601]
8. He YF, Li BZ, Li Z, Liu P, Wang Y, Tang Q, Ding J, Jia Y, Chen Z, Li L, et al. (2011). Tet-mediated formation of 5-carboxylcytosine and its excision by TDG in mammalian DNA. Science 333, 1303–1307. 10.1126/science.1210944. [PubMed: 21817016]
9. Ito S, Shen L, Dai Q, Wu SC, Collins LB, Swenberg JA, He C, and Zhang Y. (2011). Tet proteins can convert 5-methylcytosine to 5-formylcytosine and 5-carboxylcytosine. Science 333, 1300–1303. 10.1126/science.1210597. [PubMed: 21778364]
10. Hu L, Li Z, Cheng J, Rao Q, Gong W, Liu M, Shi YG, Zhu J, Wang P, and Xu Y. (2013). Crystal structure of TET2-DNA complex: insight into TET-mediated 5mC oxidation. Cell 155, 1545–1555. 10.1016/j.cell.2013.11.020. [PubMed: 24315485]
11. Moran-Crusio K, Reavie L, Shih A, Abdel-Wahab O, Ndiaye-Lobry D, Lobry C, Figueroa ME, Vasanthakumar A, Patel J, Zhao X, et al. (2011). Tet2 loss leads to increased hematopoietic stem cell self-renewal and myeloid transformation. Cancer Cell 20, 11–24. 10.1016/j.ccr.2011.06.001. [PubMed: 21723200]
12. Weissmann S, Alpermann T, Grossmann V, Kowarsch A, Nadarajah N, Eder C, Dicker F, Fasan A, Haferlach C, Haferlach T, et al. (2012). Landscape of TET2 mutations in acute myeloid leukemia. Leukemia 26, 934–942. 10.1038/leu.2011.326. [PubMed: 22116554]
13. Chou WC, Chou SC, Liu CY, Chen CY, Hou HA, Kuo YY, Lee MC, Ko BS, Tang JL, Yao M, et al. (2011). TET2 mutation is an unfavorable prognostic factor in acute myeloid leukemia patients with

intermediate-risk cytogenetics. Blood 118, 3803–3810. 10.1182/blood-2011-02-339747. [PubMed: 21828143]

14. Abdel-Wahab O, Mullally A, Hedvat C, Garcia-Manero G, Patel J, Wadleigh M, Malinge S, Yao J, Kilpivaara O, Bhat R, et al. (2009). Genetic characterization of TET1, TET2, and TET3 alterations in myeloid malignancies. Blood 114, 144–147. blood-2009–03-210039. [PubMed: 19420352]
15. Itzykson R, Kosmider O, Cluzeau T, Mansat-De Mas V, Dreyfus F, Beyne-Rauzy O, Quesnel B, Vey N, Gelsi-Boyer V, Raynaud S, et al. (2011). Impact of TET2 mutations on response rate to azacitidine in myelodysplastic syndromes and low blast count acute myeloid leukemias. Leukemia 25, 1147–1152. 10.1038/leu.2011.71. [PubMed: 21494260]
16. Morinishi L., Kochanowski K., Levine RL., Wu LF., and Altschuler SJ. (2020). Loss of TET2 Affects Proliferation and Drug Sensitivity through Altered Dynamics of Cell-State Transitions. Cell Syst 11, 86–94 e85. 10.1016/j.cels.2020.06.003. [PubMed: 32619551]
17. Shen Q, Zhang Q, Shi Y, Shi Q, Jiang Y, Gu Y, Li Z, Li X, Zhao K, Wang C, et al. (2018). Tet2 promotes pathogen infection-induced myelopoiesis through mRNA oxidation. Nature 554, 123–127. 10.1038/nature25434. [PubMed: 29364877]
18. Guallar D, Bi X, Pardavila JA, Huang X, Saenz C, Shi X, Zhou H, Faiola F, Ding J, Haruehanroengra P, et al. (2018). RNA-dependent chromatin targeting of TET2 for endogenous retrovirus control in pluripotent stem cells. Nat Genet 50, 443–451. 10.1038/s41588-018-0060-9. [PubMed: 29483655]
19. Fu L, Guerrero CR, Zhong N, Amato NJ, Liu Y, Liu S, Cai Q, Ji D, Jin SG, Niedernhofer LJ, et al. (2014). Tet-mediated formation of 5-hydroxymethylcytosine in RNA. Journal of the American Chemical Society 136, 11582–11585. 10.1021/ja505305z.
20. Lan J, Rajan N, Bizet M, Penning A, Singh NK, Guallar D, Calonne E, Li Greci A, Bonvin E, Deplus R, et al. (2020). Functional role of Tet-mediated RNA hydroxymethylcytosine in mouse ES cells and during differentiation. Nature communications 11, 4956. 10.1038/s41467-020-18729-6.
21. Yang X, Yang Y, Sun BF, Chen YS, Xu JW, Lai WY, Li A, Wang X, Bhattarai DP, Xiao W, et al. (2017). 5-methylcytosine promotes mRNA export - NSUN2 as the methyltransferase and ALYREF as an m(5)C reader. Cell research 27, 606–625. 10.1038/cr.2017.55. [PubMed: 28418038]
22. Yang Y, Wang L, Han X, Yang WL, Zhang M, Ma HL, Sun BF, Li A, Xia J, Chen J, et al. (2019). RNA 5-Methylcytosine Facilitates the Maternal-to-Zygotic Transition by Preventing Maternal mRNA Decay. Mol Cell 75, 1188–1202 e1111. 10.1016/j.molcel.2019.06.033. [PubMed: 31399345]
23. Delatte B, Wang F, Ngoc LV, Collignon E, Bonvin E, Deplus R, Calonne E, Hassabi B, Putmans P, Awe S, et al. (2016). RNA biochemistry. Transcriptome-wide distribution and function of RNA hydroxymethylcytosine. Science 351, 282–285. 10.1126/science.aac5253. [PubMed: 26816380]
24. Kantarjian H, Kadia T, DiNardo C, Daver N, Borthakur G, Jabbour E, Garcia-Manero G, Konopleva M, and Ravandi F. (2021). Acute myeloid leukemia: current progress and future directions. Blood Cancer J 11, 41. 10.1038/s41408-021-00425-3. [PubMed: 33619261]
25. Dohner H, Weisdorf DJ, and Bloomfield CD (2015). Acute Myeloid Leukemia. N Engl J Med 373, 1136–1152. 10.1056/NEJMra1406184. [PubMed: 26376137]
26. Thol F, and Ganser A. (2020). Treatment of Relapsed Acute Myeloid Leukemia. Curr Treat Options Oncol 21, 66. 10.1007/s11864-020-00765-5. [PubMed: 32601974]
27. Vetrie D., Helgason GV., and Copland M. (2020). The leukaemia stem cell: similarities, differences and clinical prospects in CML and AML. Nat Rev Cancer 20, 158–173. 10.1038/s41568-019-0230-9. [PubMed: 31907378]
28. Pollyea DA, and Jordan CT (2017). Therapeutic targeting of acute myeloid leukemia stem cells. Blood 129, 1627–1635. 10.1182/blood-2016-10-696039. [PubMed: 28159738]
29. Thomas D, and Majeti R. (2017). Biology and relevance of human acute myeloid leukemia stem cells. Blood 129, 1577–1585. 10.1182/blood-2016-10-696054. [PubMed: 28159741]
30. Tasian SK, Bornhauser M, and Rutella S. (2018). Targeting Leukemia Stem Cells in the Bone Marrow Niche. Biomedicines 6. 10.3390/biomedicines6010022.
31. Konopleva MY, and Jordan CT (2011). Leukemia stem cells and microenvironment: biology and therapeutic targeting. J Clin Oncol 29, 591–599. 10.1200/JCO.2010.31.0904. [PubMed: 21220598]

32. Zeng Z, Shi YX, Samudio IJ, Wang RY, Ling X, Frolova O, Levis M, Rubin JB, Negrin RR, Estey EH, et al. (2009). Targeting the leukemia microenvironment by CXCR4 inhibition overcomes resistance to kinase inhibitors and chemotherapy in AML. Blood 113, 6215–6224. 10.1182/blood-2008-05-158311. [PubMed: 18955566]
33. Pan F, Wingo TS, Zhao Z, Gao R, Makishima H, Qu G, Lin L, Yu M, Ortega JR, Wang J, et al. (2017). Tet2 loss leads to hypermutagenicity in haematopoietic stem/progenitor cells. Nat Commun 8, 15102. 10.1038/ncomms15102. [PubMed: 28440315]
34. Ko M, Huang Y, Jankowska AM, Pape UJ, Tahiliani M, Bandukwala HS, An J, Lamperti ED, Koh KP, Ganetzky R, et al. (2010). Impaired hydroxylation of 5-methylcytosine in myeloid cancers with mutant TET2. Nature 468, 839–843. 10.1038/nature09586. [PubMed: 21057493]
35. Li Z, Cai X, Cai CL, Wang J, Zhang W, Petersen BE, Yang FC, and Xu M. (2011). Deletion of Tet2 in mice leads to dysregulated hematopoietic stem cells and subsequent development of myeloid malignancies. Blood 118, 4509–4518. 10.1182/blood-2010-12-325241. [PubMed: 21803851]
36. Zhao H, Lu J, Yan T, Han F, Sun J, Yin X, Chen L, Shen C, Wunderlich M, Yun W, et al. (2022). Opioid receptor signaling suppresses leukemia through both catalytic and non-catalytic functions of TET2. Cell Rep 38, 110253. 10.1016/j.celrep.2021.110253.
37. Hatlen MA, Arora K, Vacic V, Grabowska EA, Liao W, Riley-Gillis B, Oschwald DM, Wang L, Joergens JE, Shih AH, et al. (2016). Integrative genetic analysis of mouse and human AML identifies cooperating disease alleles. The Journal of experimental medicine 213, 25–34. 10.1084/jem.20150524. [PubMed: 26666262]
38. Bagger FO, Kinalis S, and Rapin N. (2019). BloodSpot: a database of healthy and malignant haematopoiesis updated with purified and single cell mRNA sequencing profiles. Nucleic Acids Res 47, D881–D885. 10.1093/nar/gky1076. [PubMed: 30395307]
39. Tyner JW., Tognon CE., Bottomly D., Wilmot B., Kurtz SE., Savage SL., Long N., Schultz AR., Traer E., Abel M., et al. . (2018). Functional genomic landscape of acute myeloid leukaemia. Nature 562, 526–531. 10.1038/s41586-018-0623-z. [PubMed: 30333627]
40. van Galen P, Hovestadt V, Wadsworth Ii MH, Hughes TK, Griffin GK, Battaglia S, Verga JA, Stephansky J, Pastika TJ, Lombardi Story J, et al. (2019). Single-Cell RNA-Seq Reveals AML Hierarchies Relevant to Disease Progression and Immunity. Cell 176, 1265–1281 e1224. 10.1016/j.cell.2019.01.031. [PubMed: 30827681]
41. Yan M, Kanbe E, Peterson LF, Boyapati A, Miao Y, Wang Y, Chen IM, Chen Z, Rowley JD, Willman CL, and Zhang DE (2006). A previously unidentified alternatively spliced isoform of t(8;21) transcript promotes leukemogenesis. Nat Med 12, 945–949. [PubMed: 16892037]
42. Krivtsov AV, Twomey D, Feng Z, Stubbs MC, Wang Y, Faber J, Levine JE, Wang J, Hahn WC, Gilliland DG, et al. (2006). Transformation from committed progenitor to leukaemia stem cell initiated by MLL-AF9. Nature 442, 818–822. 10.1038/nature04980. [PubMed: 16862118]
43. Boyerinas B, Zafrir M, Yesilkanal AE, Price TT, Hyjek EM, and Sipkins DA (2013). Adhesion to osteopontin in the bone marrow niche regulates lymphoblastic leukemia cell dormancy. Blood 121, 4821–4831. 10.1182/blood-2012-12-475483. [PubMed: 23589674]
44. Ko M, Bandukwala HS, An J, Lamperti ED, Thompson EC, Hastie R, Tsangaratou A, Rajewsky K, Koralov SB, and Rao A. (2011). Ten-Eleven-Translocation 2 (TET2) negatively regulates homeostasis and differentiation of hematopoietic stem cells in mice. Proceedings of the National Academy of Sciences of the United States of America 108, 14566–14571. 10.1073/pnas.1112317108. [PubMed: 21873190]
45. Balise VD, Saito-Reis CA, and Gillette JM (2020). Tetraspanin Scaffold Proteins Function as Key Regulators of Hematopoietic Stem Cells. Front Cell Dev Biol 8, 598. 10.3389/fcell.2020.00598. [PubMed: 32754593]
46. Kwon HY, Bajaj J, Ito T, Blevins A, Konuma T, Weeks J, Lytle NK, Koechlein CS, Rizzieri D, Chuah C, et al. (2015). Tetraspanin 3 Is Required for the Development and Propagation of Acute Myelogenous Leukemia. Cell Stem Cell 17, 152–164. 10.1016/j.stem.2015.06.006. [PubMed: 26212080]
47. Marjon KD, Termini CM, Karlen KL, Saito-Reis C, Soria CE, Lidke KA, and Gillette JM (2016). Tetraspanin CD82 regulates bone marrow homing of acute myeloid leukemia by modulating

the molecular organization of N-cadherin. Oncogene 35, 4132–4140. 10.1038/onc.2015.449. [PubMed: 26592446]

48. Saito-Reis CA, Marjon KD, Pascetti EM, Floren M, and Gillette JM (2018). The tetraspanin CD82 regulates bone marrow homing and engraftment of hematopoietic stem and progenitor cells. Mol Biol Cell 29, 2946–2958. 10.1091/mbc.E18-05-0305. [PubMed: 30133344]
49. Mousavi A. (2020). CXCL12/CXCR4 signal transduction in diseases and its molecular approaches in targeted-therapy. Immunol Lett 217, 91–115. 10.1016/j.imlet.2019.11.007. [PubMed: 31747563]
50. Cancilla D, Rettig MP, and DiPersio JF (2020). Targeting CXCR4 in AML and ALL. Frontiers in oncology 10, 1672. 10.3389/fonc.2020.01672. [PubMed: 33014834]
51. Leung KT, Chan KY, Ng PC, Lau TK, Chiu WM, Tsang KS, Li CK, Kong CK, and Li K. (2011). The tetraspanin CD9 regulates migration, adhesion, and homing of human cord blood CD34+ hematopoietic stem and progenitor cells. Blood 117, 1840–1850. 10.1182/blood-2010-04-281329. [PubMed: 21063023]
52. Yoshida N, Kitayama D, Arima M, Sakamoto A, Inamine A, Watanabe-Takano H, Hatano M, Koike T, and Tokuhisa T. (2011). CXCR4 expression on activated B cells is downregulated by CD63 and IL-21. J Immunol 186, 2800–2808. 10.4049/jimmunol.1003401. [PubMed: 21270405]
53. Rasmussen KD, Jia G, Johansen JV, Pedersen MT, Rapin N, Bagger FO, Porse BT, Bernard OA, Christensen J, and Helin K. (2015). Loss of TET2 in hematopoietic cells leads to DNA hypermethylation of active enhancers and induction of leukemogenesis. Genes & development 29, 910–922. 10.1101/gad.260174.115. [PubMed: 25886910]
54. Legrand C, Tuorto F, Hartmann M, Liebers R, Jacob D, Helm M, and Lyko F. (2017). Statistically robust methylation calling for whole-transcriptome bisulfite sequencing reveals distinct methylation patterns for mouse RNAs. Genome research 27, 1589–1596. 10.1101/gr.210666.116. [PubMed: 28684555]
55. Huang Y, Su R, Sheng Y, Dong L, Dong Z, Xu H, Ni T, Zhang ZS, Zhang T, Li C, et al. (2019). Small-Molecule Targeting of Oncogenic FTO Demethylase in Acute Myeloid Leukemia. Cancer Cell 35, 677–691 e610. 10.1016/j.ccell.2019.03.006. [PubMed: 30991027]
56. Qing Y, Su R, and Chen J. (2021). RNA modifications in hematopoietic malignancies: a new research frontier. Blood 138, 637–648. 10.1182/blood.2019004263. [PubMed: 34157073]
57. Huang H, Weng H, and Chen J. (2020). m(6)A Modification in Coding and Non-coding RNAs: Roles and Therapeutic Implications in Cancer. Cancer Cell 37, 270–288. 10.1016/j.ccell.2020.02.004. [PubMed: 32183948]
58. He C, Sidoli S, Warneford-Thomson R, Tatomer DC, Wilusz JE, Garcia BA, and Bonasio R. (2016). High-Resolution Mapping of RNA-Binding Regions in the Nuclear Proteome of Embryonic Stem Cells. Mol Cell 64, 416–430. 10.1016/j.molcel.2016.09.034. [PubMed: 27768875]
59. He C, Bozler J, Janssen KA, Wilusz JE, Garcia BA, Schorn AJ, and Bonasio R. (2021). TET2 chemically modifies tRNAs and regulates tRNA fragment levels. Nat Struct Mol Biol 28, 62–70. 10.1038/s41594-020-00526-w. [PubMed: 33230319]
60. Shen H, Ontiveros RJ, Owens MC, Liu MY, Ghanty U, Kohli RM, and Liu KF (2021). TET-mediated 5-methylcytosine oxidation in tRNA promotes translation. J Biol Chem 296, 100087. 10.1074/jbc.RA120.014226. [PubMed: 33199375]
61. Grozhik AV., Olarerin-George AO., Sindelar M., Li X., Gross SS., and Jaffrey SR. (2019). Antibody cross-reactivity accounts for widespread appearance of m(1)A in 5'UTRs. Nat Commun 10, 5126. 10.1038/s41467-019-13146-w. [PubMed: 31719534]
62. Zhang LS, Liu C, Ma H, Dai Q, Sun HL, Luo G, Zhang Z, Zhang L, Hu L, Dong X, and He C. (2019). Transcriptome-wide Mapping of Internal N(7)-Methylguanosine Methylome in Mammalian mRNA. Mol Cell 74, 1304–1316 e1308. 10.1016/j.molcel.2019.03.036. [PubMed: 31031084]
63. Su R, Dong L, Li C, Nachtergaele S, Wunderlich M, Qing Y, Deng X, Wang Y, Weng X, Hu C, et al. (2018). R-2HG Exhibits Anti-tumor Activity by Targeting FTO/m(6)A/MYC/CEBPA Signaling. Cell 172, 90–105 e123. 10.1016/j.cell.2017.11.031. [PubMed: 29249359]

64. Ganzel C, Sun Z, Cripe LD, Fernandez HF, Douer D, Rowe JM, Paietta EM, Ketterling R, O'Connell MJ, Wiernik PH, et al. (2018). Very poor long-term survival in past and more recent studies for relapsed AML patients: The ECOG-ACRIN experience. Am J Hematol 93, 1074–1081. 10.1002/ajh.25162. [PubMed: 29905379]

65. Yates JW, Wallace HJ Jr., Ellison RR, and Holland JF (1973). Cytosine arabinoside (NSC-63878) and daunorubicin (NSC-83142) therapy in acute nonlymphocytic leukemia. Cancer Chemother Rep 57, 485–488. [PubMed: 4586956]

66. Cucchi DGJ, Groen RWJ, Janssen J, and Cloos J. (2020). Ex vivo cultures and drug testing of primary acute myeloid leukemia samples: Current techniques and implications for experimental design and outcome. Drug Resist Updat 53, 100730. 10.1016/j.drup.2020.100730.

67. Agarwal P, Isringhausen S, Li H, Paterson AJ, He J, Gomariz A, Nagasawa T, Nombela-Arrieta C, and Bhatia R. (2019). Mesenchymal Niche-Specific Expression of Cxcl12 Controls Quiescence of Treatment-Resistant Leukemia Stem Cells. Cell Stem Cell 24, 769–784 e766. 10.1016/j.stem.2019.02.018. [PubMed: 30905620]

68. Nervi B, Ramirez P, Rettig MP, Uy GL, Holt MS, Ritchey JK, Prior JL, Piwnica-Worms D, Bridger G, Ley TJ, and DiPersio JF (2009). Chemosensitization of acute myeloid leukemia (AML) following mobilization by the CXCR4 antagonist AMD3100. Blood 113, 6206–6214. 10.1182/blood-2008-06-162123. [PubMed: 19050309]

69. Camp RL, Dolled-Filhart M, and Rimm DL (2004). X-tile: a new bio-informatics tool for biomarker assessment and outcome-based cut-point optimization. Clin Cancer Res 10, 7252–7259. [PubMed: 15534099]

70. Wang Y, and Zhang Y. (2014). Regulation of TET protein stability by calpains. Cell Rep 6, 278–284. 10.1016/j.celrep.2013.12.031. [PubMed: 24412366]

71. Kazi JU., Sun J., Phung B., Zadjali F., Flores-Morales A., and Ronnstrand L. (2012). Suppressor of cytokine signaling 6 (SOCS6) negatively regulates Flt3 signal transduction through direct binding to phosphorylated tyrosines 591 and 919 of Flt3. J Biol Chem 287, 36509–36517. 10.1074/jbc.M112.376111.

72. Campeau E, Ruhl VE, Rodier F, Smith CL, Rahmberg BL, Fuss JO, Campisi J, Yaswen P, Cooper PK, and Kaufman PD (2009). A versatile viral system for expression and depletion of proteins in mammalian cells. PloS one 4, e6529. 10.1371/journal.pone.0006529.

73. Stewart SA, Dykxhoorn DM, Palliser D, Mizuno H, Yu EY, An DS, Sabatini DM, Chen IS, Hahn WC, Sharp PA, et al. (2003). Lentivirus-delivered stable gene silencing by RNAi in primary cells. RNA 9, 493–501. 10.1261/rna.2192803. [PubMed: 12649500]

74. Naviaux RK, Costanzi E, Haas M, and Verma IM (1996). The pCL vector system: rapid production of helper-free, high-titer, recombinant retroviruses. J Virol 70, 5701–5705. 10.1128/JVI.70.8.5701-5705.1996. [PubMed: 8764092]

75. Li B, and Dewey CN (2011). RSEM: accurate transcript quantification from RNA-Seq data with or without a reference genome. BMC Bioinformatics 12, 323. 10.1186/1471-2105-12-323. [PubMed: 21816040]

76. Dobin A, Davis CA, Schlesinger F, Drenkow J, Zaleski C, Jha S, Batut P, Chaisson M, and Gingeras TR (2013). STAR: ultrafast universal RNA-seq aligner. Bioinformatics 29, 15–21. 10.1093/bioinformatics/bts635. [PubMed: 23104886]

77. Thorvaldsdottir H, Robinson JT, and Mesirov JP (2013). Integrative Genomics Viewer (IGV): high-performance genomics data visualization and exploration. Brief Bioinform 14, 178–192. 10.1093/bib/bbs017. [PubMed: 22517427]

78. Subramanian A, Tamayo P, Mootha VK, Mukherjee S, Ebert BL, Gillette MA, Paulovich A, Pomeroy SL, Golub TR, Lander ES, and Mesirov JP (2005). Gene set enrichment analysis: a knowledge-based approach for interpreting genome-wide expression profiles. Proceedings of the National Academy of Sciences of the United States of America 102, 15545–15550. 10.1073/pnas.0506580102. [PubMed: 16199517]

79. He B, Li X, Hu T, Lian W, and Zhang M. (2017). Construction of a lentiviral vector containing shRNA targeting ADAM17 and its role in attenuating endotoxemia in mice. Mol Med Rep 16, 6013–6019. 10.3892/mmr.2017.7307. [PubMed: 28849138]

80. Su R, Dong L, Li Y, Gao M, He PC, Liu W, Wei J, Zhao Z, Gao L, Han L, et al. (2022). METTL16 exerts an m(6)A-independent function to facilitate translation and tumorigenesis. Nat Cell Biol 24, 205–216. 10.1038/s41556-021-00835-2. [PubMed: 35145225]
81. Shen C, Sheng Y, Zhu AC, Robinson S, Jiang X, Dong L, Chen H, Su R, Yin Z, Li W, et al. (2020). RNA Demethylase ALKBH5 Selectively Promotes Tumorigenesis and Cancer Stem Cell Self-Renewal in Acute Myeloid Leukemia. Cell Stem Cell 27, 64–80 e69. 10.1016/j.stem.2020.04.009. [PubMed: 32402250]
82. Su R., Dong L., Li Y., Gao M., Han L., Wunderlich M., Deng X., Li H., Huang Y., Gao L., et al. . (2020). Targeting FTO Suppresses Cancer Stem Cell Maintenance and Immune Evasion. Cancer cell 38, 79–96 e11. 10.1016/j.ccell.2020.04.017. [PubMed: 32531268]
83. Han L, Dong L, Leung K, Zhao Z, Li Y, Gao L, Chen Z, Xue J, Qing Y, Li W, et al. (2023). METTL16 drives leukemogenesis and leukemia stem cell self-renewal by reprogramming BCAA metabolism. Cell Stem Cell 30, 52–68 e13. 10.1016/j.stem.2022.12.006. [PubMed: 36608679]
84. He X, Wan J, Yang X, Zhang X, Huang D, Li X, Zou Y, Chen C, Yu Z, Xie L, et al. (2021). Bone marrow niche ATP levels determine leukemia-initiating cell activity via P2X7 in leukemic models. J Clin Invest 131. 10.1172/JCI140242.
85. Hu Y, and Smyth GK (2009). ELDA: extreme limiting dilution analysis for comparing depleted and enriched populations in stem cell and other assays. J Immunol Methods 347, 70–78. 10.1016/j.jim.2009.06.008. [PubMed: 19567251]
86. Hao X, Gu H, Chen C, Huang D, Zhao Y, Xie L, Zou Y, Shu HS, Zhang Y, He X, et al. (2019). Metabolic Imaging Reveals a Unique Preference of Symmetric Cell Division and Homing of Leukemia-Initiating Cells in an Endosteal Niche. Cell metabolism 29, 950–965 e956. 10.1016/j.cmet.2018.11.013. [PubMed: 30581117]
87. Zhang B, Nguyen LXT, Zhao D, Frankhouser DE, Wang H, Hoang DH, Qiao J, Abundis C, Brehove M, Su YL, et al. (2021). Treatment-induced arteriolar revascularization and miR-126 enhancement in bone marrow niche protect leukemic stem cells in AML. J Hematol Oncol 14, 122. 10.1186/s13045-021-01133-y. [PubMed: 34372909]
88. Quinlivan EP, and Gregory JF 3rd (2008). DNA digestion to deoxyribonucleoside: a simplified one-step procedure. Analytical biochemistry 373, 383–385. 10.1016/j.ab.2007.09.031. [PubMed: 18028864]
89. Wang X, Lu Z, Gomez A, Hon GC, Yue Y, Han D, Fu Y, Parisien M, Dai Q, Jia G, et al. (2014). N6-methyladenosine-dependent regulation of messenger RNA stability. Nature 505, 117–120. 10.1038/nature12730. [PubMed: 24284625]
90. Martin M.J.E.j. (2011). Cutadapt removes adapter sequences from high-throughput sequencing reads. 17, 10–12.
91. Rieder D, Amort T, Kugler E, Lusser A, and Trajanoski Z. (2016). meRanTK: methylated RNA analysis ToolKit. Bioinformatics 32, 782–785. 10.1093/bioinformatics/btv647. [PubMed: 26543174]
92. Chen X., Li A., Sun BF., Yang Y., Han YN., Yuan X., Chen RX., Wei WS., Liu Y., Gao CC., et al. . (2019). 5-methylcytosine promotes pathogenesis of bladder cancer through stabilizing mRNAs. Nat Cell Biol 21, 978–990. 10.1038/s41556-019-0361-y. [PubMed: 31358969]

## Highlights

- Microenvironment is crucial for *TET2* deficiency-induced fast leukemogenesis *in vivo*
- *TET2* loss promotes LSC homing into BM niche and thereby increases LSC self-renewal
- *TET2* loss activates the TSPAN13/CXCR4 axis to facilitate LSC homing
- TET2 post-transcriptionally inhibits *TSPAN13* expression as an mRNA $m^5C$ eraser

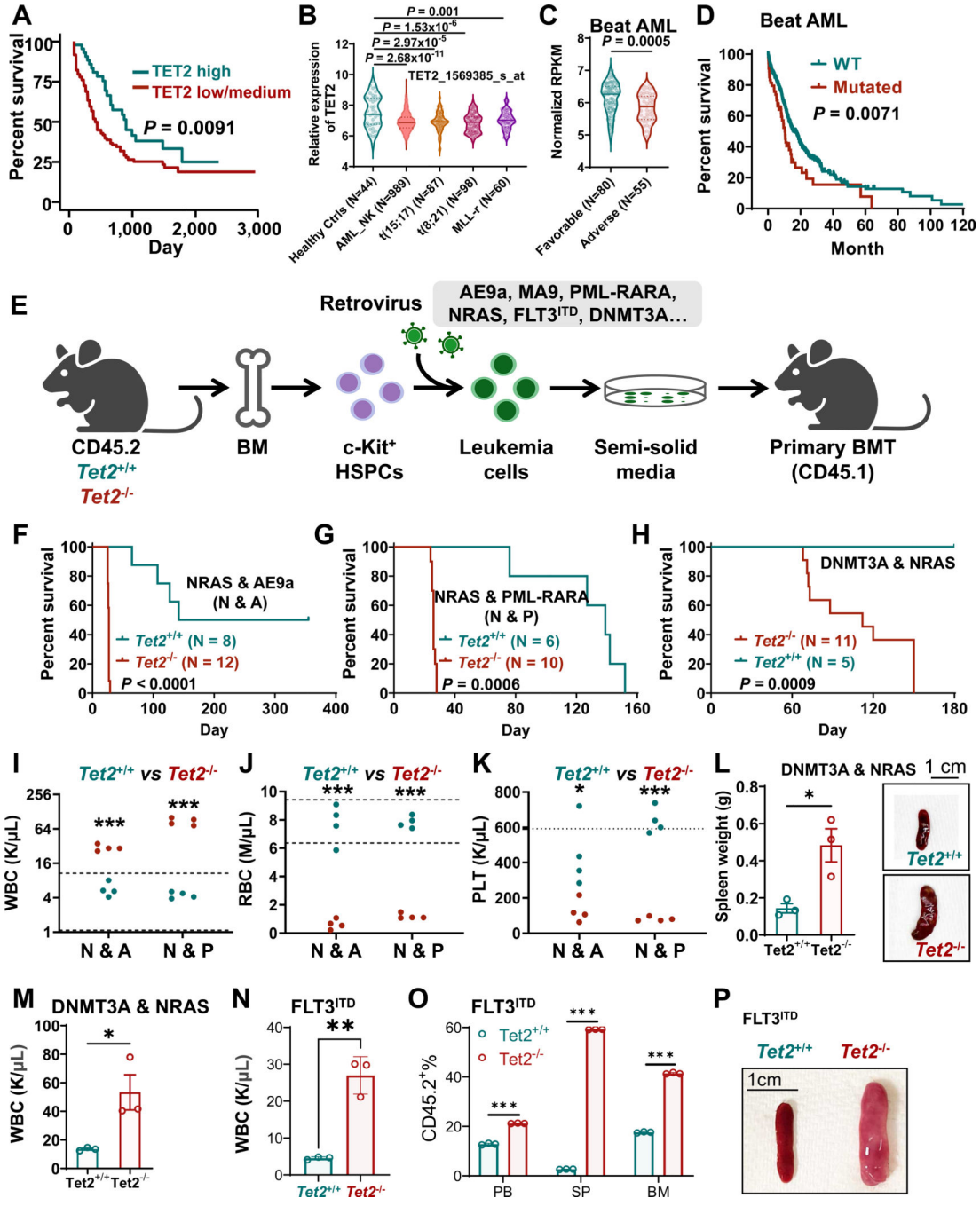


**Figure 1. *TET2* deficiency predicts poor prognosis in AML patients and promotes primary leukemogenesis.**

(A) Kaplan-Meier survival curves of TCGA AML patients TET2 high (n=44; roughly the top 1/4) and low/medium (n=119; the remaining patients) expression. The X-tile software [69] was used to determine the optimal cutoff values for predicting survival.

(B) Violin plots showing the expression of *TET2* in healthy donors and AML patients. The expression values, derived from Affymetrix exon arrays, were $\log_2$ transformed.

(C) Violin plots showing the relative expression of *TET2* in favorable and adverse AML patients in the Beat AML cohort.

(D) Kaplan-Meier survival curves of AML patients with or without TET2 mutation. WT, wild-type (without *TET2* mutation in the Beat AML cohort, http://vizome.org/aml/). n = 54 for TET2 mutation group; n = 415 for TET2 WT group.

(E) Schematic outline of primary BMT models driven by various gene mutations and translocations.

(F-H) Kaplan-Meier survival curves of $NRAS^{mut}$ & AE9a (F), $NRAS^{mut}$ & PML-RARA (G), and $DNMT3A^{mut}$ & $NRAS^{mut}$ (H)-driven primary murine AML models upon *Tet2* deficiency. *Tet2* (ΔE8–10) strain was used for F and G; *Tet2* (ΔE3) strain was used for H.

(I-K) The white blood cell (WBC) count (I), red blood cell (RBC) count (J), and platelet (PLT) count (K) in the recipient mice transplanted with $Tet2^{+/+}$ versus $Tet2^{-/-}$ (ΔE8–10) primary NRAS/AE9a (N&A) or NRAS/PML-RARA (N&P) cells (n = 4).

(L) The spleen weight and representative spleens of $DNMT3A^{mut}$ & $NRAS^{mut}$ -driven primary murine AML models (n = 3).

(M and N) The WBC count in the recipient mice transplanted with primary $DNMT3A^{mut}$ & $NRAS^{mut}$ (M)- or $FLT3^{ITD}$ (N)-transformed $Tet^{+/+}$ or $Tet2^{-/-}$ mouse BM progenitor cells (n = 3).

(O) Effect of *Tet2* deficiency on the engraftment of $FLT3^{ITD}$ leukemia cells into peripheral blood (PB), spleen (SP), and BM of primary recipient mice. The samples were collected on day 52 post transplantation (n = 3).

(P) The representative spleens of $FLT3^{ITD}$-driven primary murine AML models. The samples were collected on day 52 post transplantation.

Unpaired two-tailed Student's t-test (B, C, and I-O); log-rank test (A, D, and F-H); *p < 0.05, **p < 0.01, ***p < 0.001.

See also Figures S1.

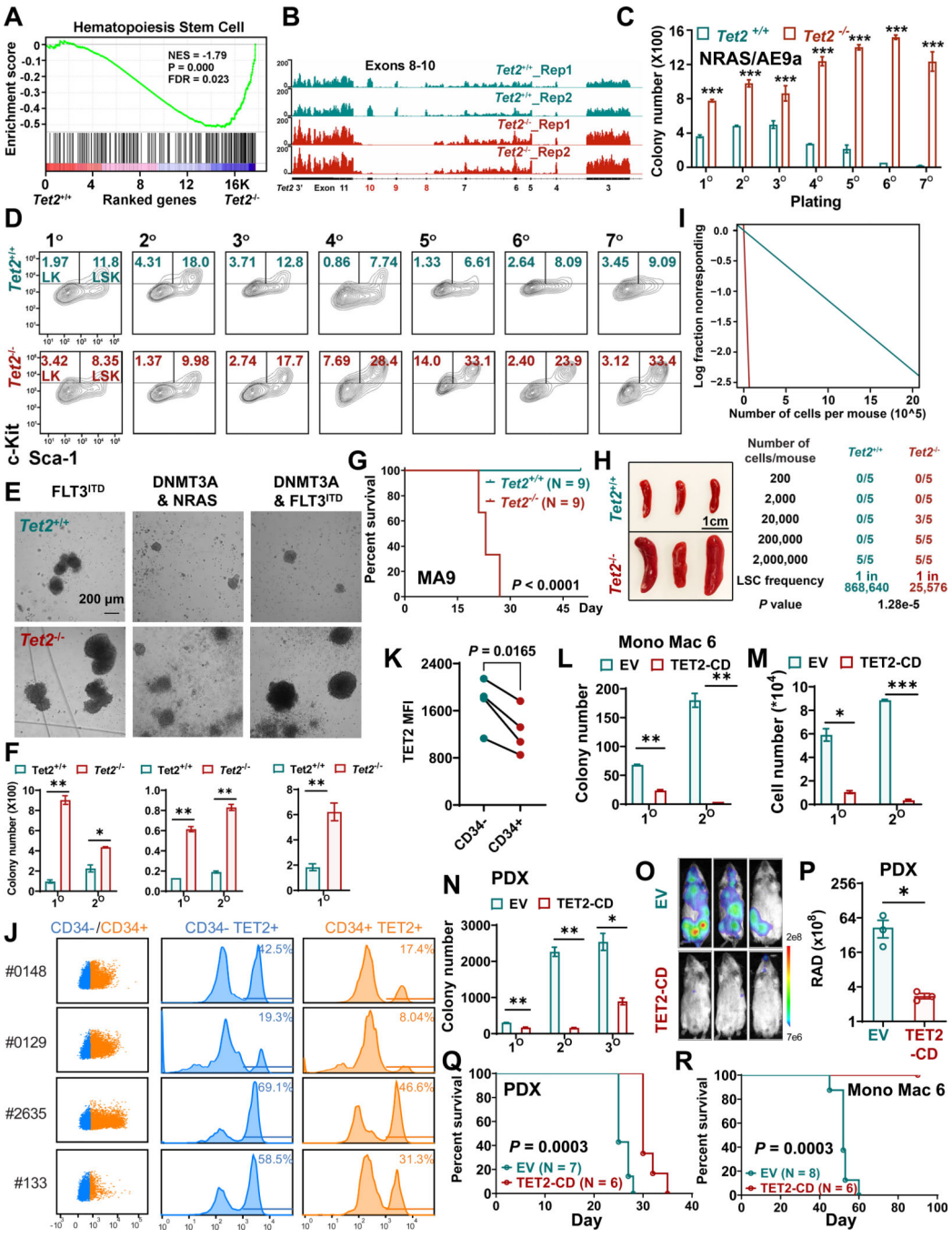


**Figure 2. *Tet2* depletion significantly enhances LSC self-renewal while its overexpression attenuates LSC self-renewal and AML progression in various models.**

(A) Enrichment plot of Ivanova hematopoiesis stem cell pathway which was activated in *Tet2*$^{-/-}$ (ΔE8–10) primary NRAS/AE9a AML cells.

(B) IGV tracks of *Tet2* in *Tet2*$^{+/+}$ or *Tet2*$^{-/-}$ (ΔE8–10) NRAS/AE9a AML cells.

(C) Colony numbers from serial replating assays with *Tet2*$^{+/+}$ and *Tet2*$^{-/-}$ (ΔE3) primary leukemia cells. The representative data from NRAS/AE9a model was shown.

(D) FACS plots depicting the percentage of LK (Lin$^{-}$c-Kit$^{+}$Sca-1$^{-}$) and LSK (Lin$^{-}$c-Kit$^{+}$Sca-1$^{+}$) subpopulations in *Tet2*$^{+/+}$ and *Tet2*$^{-/-}$ (ΔE3) NRAS/AE9a AML cells.

(E) The representative colony images of *Tet2* $^{+/+}$ or *Tet2* $^{-/-}$ (ΔE3) primary AML cells driven by FLT3$^{ITD}$, DNMT3A$^{mut}$ & NRAS$^{mut}$, and DNMT3A$^{mut}$ & FLT3$^{ITD}$.
(F) Effect of *Tet2* depletion on the colony numbers of primary AML cells driven by FLT3$^{ITD}$ (left), DNMT3A$^{mut}$ & NRAS$^{mut}$ (middle), and DNMT3A$^{mut}$ & FLT3$^{ITD}$ (right).
(G) Kaplan-Meier survival curves of secondary BMT recipient mice. The leukemic BM cells isolated from the primary BMT recipient mice of *Tet2*$^{+/+}$ + MA9 or *Tet2*$^{-/-}$ (ΔE8–10) + MA9 were used as donor cells.
(H) Representative spleen images of the secondary BMT models. All the spleens were collected on day 27 post transplantation of *Tet2*$^{+/+}$ + MA9 or *Tet2*$^{-/-}$ (ΔE8–10) + MA9 primary AML cells.
(I) The *in vivo* limiting dilution assay with *Tet2*$^{+/+}$ + MA9 or *Tet2*$^{-/-}$ (ΔE8–10) + MA9 primary BM leukemia cells. CD45.2 recipients (n = 5 for each group) were transplanted with different doses of leukemia cells and the estimated LSC frequencies were displayed.
(J) TET2 protein levels in the CD34$^{+}$ and CD34$^{-}$ populations of primary AML patient samples as determined by intracellular staining.
(K) Comparison of mean fluorescence intensity (MFI) of TET2 protein levels between CD34$^{+}$ and CD34$^{-}$ populations in primary AML patient samples.
(L-M) Effect of TET2 overexpression on the colony number (L) and cell number (M) of Mono Mac 6 AML cells.
(N) Effect of TET2 overexpression on the colony number of AML PDX (PDX-148, carrying DNMT3A mutation) cells.
(O) The bioluminescence images of AML PDX model (PDX-129, carrying a complex karyotype) with or without TET2 overexpression. The images were photted on day 25 post transplantation.
(P) The statistical bioluminescence signals of AML PDX model with or without TET2 overexpression.
(Q) Kaplan-Meier survival curves of AML PDX models with or without TET2 overexpression.
(R) Kaplan-Meier survival curves of Mono Mac 6-induced AML xenograft models with or without TET2 overexpression.
Unpaired two-tailed Student’s t-test (C, F, L-N, and P); log-rank test (G, Q, and R); paired two-tailed Student’s t-test (K); *p < 0.05, **p < 0.01, ***p < 0.001.
See also Figures S2 and S3.

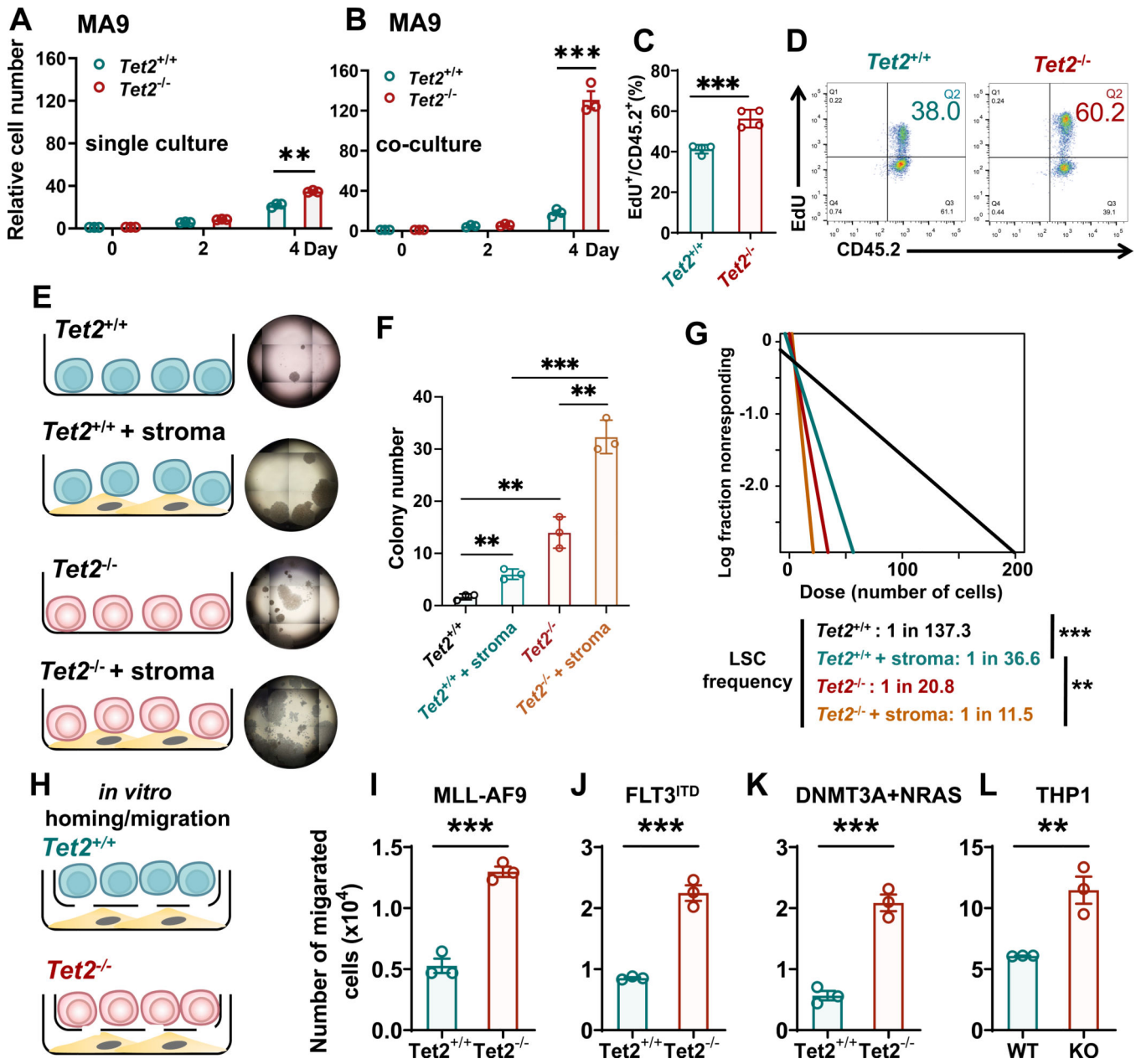


**Figure 3. *Tet2* deficiency promotes the migration of AML blast cells or LSCs into surrounding stroma to maintain their self-renewal.**

(A-B) Effect of *Tet2* depletion on the proliferation of primary MA9 cells in single culture condition (A) and stroma cell (OP-9) co-culture condition (B). The numbers of days after culture or co-culture are indicated under the x-axis.

(C-D) The effect of *Tet2* deficiency on the proliferation of MA9-transformed leukemic cells after co-culturing with OP9 stromal cells for 8 days, as determined by 5-ethynyl-2′-deoxyuridine (EdU) staining. C, the statistical results of the percentage of EdU positive cells; D, representative flow cytometry data.

(E) Scheme showing the single culture and co-culture of primary AML cells with OP-9 stromal cells before colony-forming assay (left) as well as the representative colony images

(right). The AML cells were co-cultured with OP-9 cells for 5 days before colony-forming assay. For each group, 150 AML cells were seeded into 96-well plate.

(F-G) The colony number (F) and LSC frequency (G, *in vitro* LDA) of *Tet2*$^{+/+}$ and *Tet2*$^{-/-}$ primary MA9 AML cells with or without co-culture.

(H) Scheme showing the transwell assay to evaluate the migration ability of *Tet2*$^{+/+}$ and *Tet2*$^{-/-}$ primary AML cells.

(I-K) The effect of *Tet2* deficiency on the migration ability of primary AML cells carrying MA9 (I), FLT3$^{ITD}$ (J), and DNMT3A & NRAS mutations (K).

(L) Effect of *TET2* KO on the migration ability of THP1 AML cells.

Unpaired two-tailed Student's t-test (A-C, F, and I-L); **p < 0.01, ***p < 0.001.

See also Figures S4.

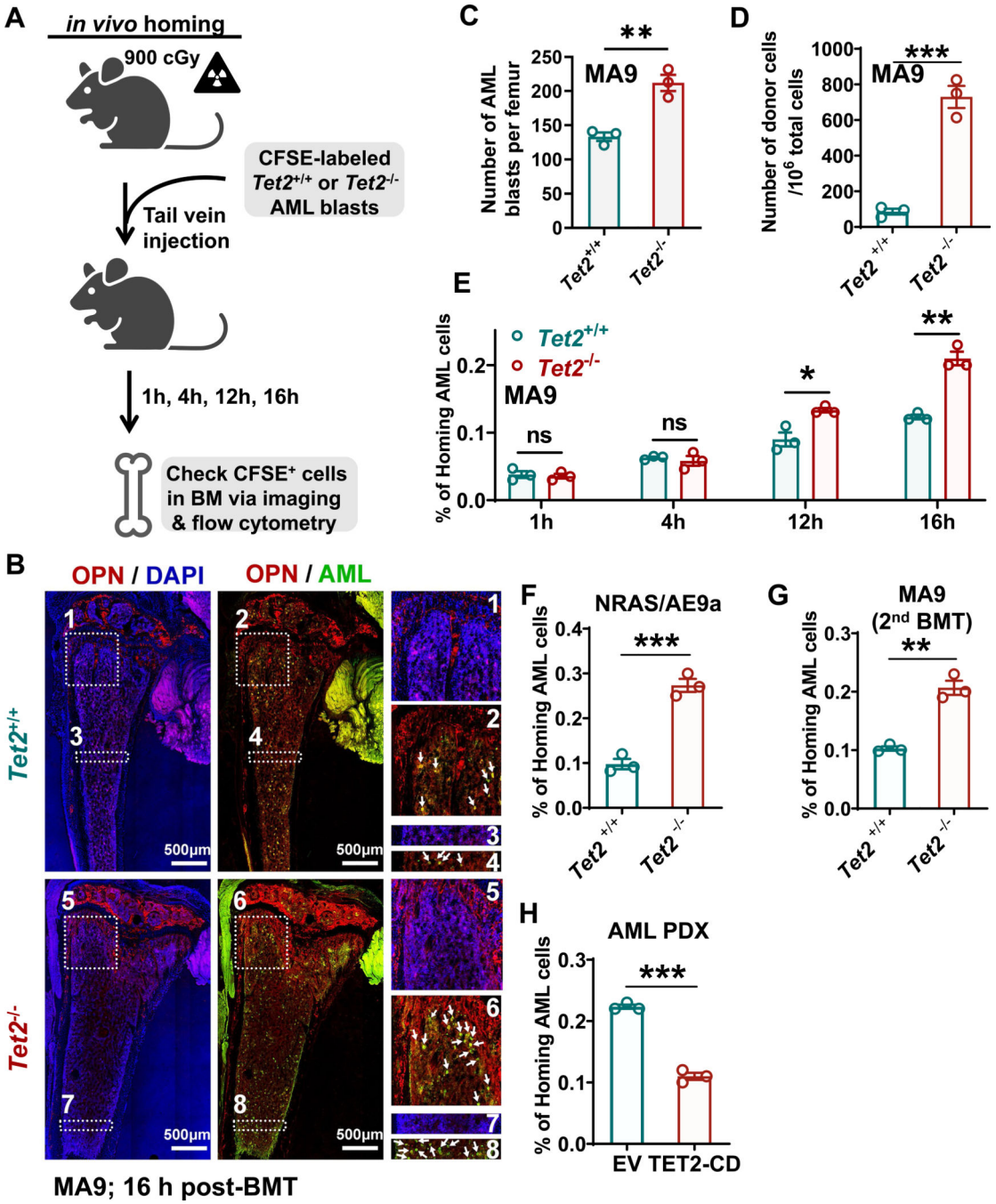


**Figure 4. *Te2* depletion facilitates LSC homing *in vivo*.**

(A) Schematic outline of the method to evaluate LSC homing *in vivo*.

(B) The *in situ* immunofluorescence (IF) of MA9 primary leukemia cells (CFSE-labeled; Green) and BM osteoblasts (Osteopontin, OPN; Red) in the femurs from *Tet2*$^{+/+}$ and *Tet2*$^{-/-}$ (ΔE8–10) group. While arrows indicated CFSE-labeled leukemia cells. The samples were collected at 16 hours post transplantation.

(C) Quantitative and statistical analysis of *in situ* IF images in Figure 4B.

(D) Effect of *Tet2* depletion on the homing of primary MA9 AML cells into the BM of recipient mice. The data were determined by flow cytometry. The samples were collected at 16 hours post transplantation.

(E) Comparison of the percentage between $Tet2^{-/-}$ and $Tet2^{+/+}$ primary MA9 AML cells homing into BM of recipient mice via flow cytometry. The samples were collected at 1, 4, 12, and 16 hours post transplantation.

(F) Effect of *Tet2* depletion on the homing of primary NRAS/AE9a AML cells. The data were determined by flow cytometry. The samples were collected at 16 hours post transplantation.

(G) Evaluation of effect of *Tet2* depletion on homing via secondary MA9 BMT models. The samples were collected at 16 hours post transplantation.

(H) Effect of TET2 overexpression on the homing of AML PDX cells into the BM of NRGS recipient mice. The samples were collected at 16 hours post transplantation.

For C-H, data were presented as mean ± SEM (n = 3). ns, not significant; *p < 0.05, **p < 0.01, ***p < 0.001; unpaired two-tailed Student's t test.

See also Figures S5.

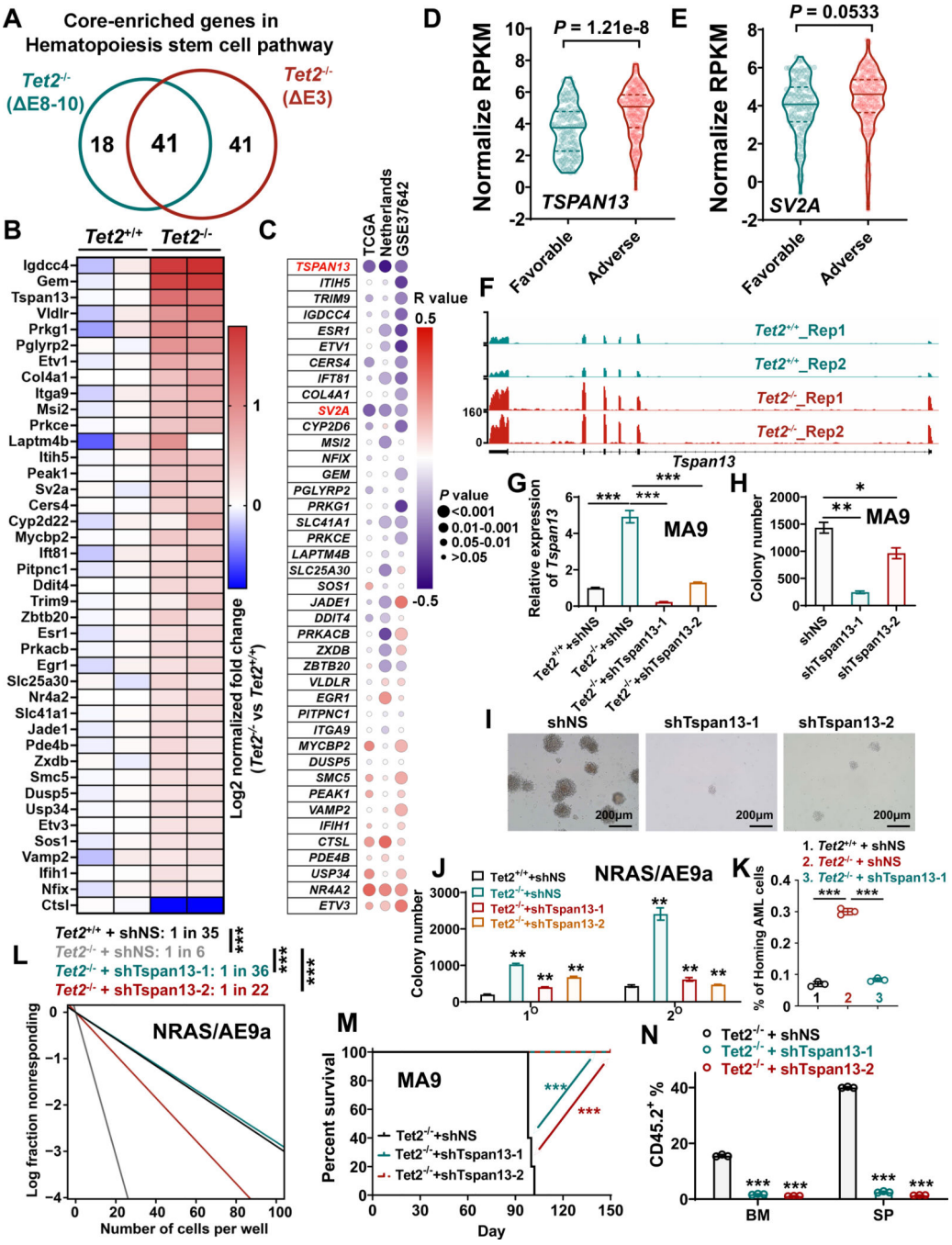


**Figure 5. Identification of *Tspan13* as a functional essential target of Tet2.**

(A) Overlap of core enriched genes in Ivanova hematopoiesis stem cell pathway from two *Tet2* KO (*Tet2*$^{-/-}$ (ΔE8–10) and *Tet2*$^{-/-}$ (ΔE3)) NRAS/AE9a AML models. The two *Tet2*$^{-/-}$ NRAS/AE9a (i.e., *Tet2*$^{-/-}$ (ΔE8–10) NRAS/AE9a and *Tet2*$^{-/-}$ (ΔE3) NRAS/AE9a) AML models as well as their corresponding control cells (*Tet2*$^{+/+}$) were subjected to RNA-seq. The left circle (green) indicates the core-enriched genes in the Ivanova hematopoiesis stem cell pathway when comparing *Tet2*$^{-/-}$ (ΔE8–10) NRAS/AE9a AML cells with their control

cells; while the right circle (red) indicates the core-enriched genes in the same pathway when comparing *Tet2*$^{-/-}$ (ΔE3) NRAS/AE9a AML cells with their control cells.
(B) Heatmap of expression level changes of the 41 overlapped core enriched genes in Ivanova hematopoiesis stem cell pathway upon *Tet2* depletion (ΔE8–10) in the NRAS/AE9a AML model.
(C) Bubble plot depicting the correlation between TET2 expression and the 41 overlapped genes in 3 human AML datasets.
(D and E) Expression levels of *TSPAN13* (D) and *SV2A* (E) in the favorable and adverse AML patients. The raw data were derived from the Beat AML cohort (http://vizome.org/aml/). The three lines inside the violin plots are the first quartile, median and third quartile; unpaired two-tailed Student's t-test.
(F) IGV track showing the abundance of *Tspan13* in *Tet2*$^{+/+}$ or *Tet2*$^{-/-}$ (ΔE3) NRAS/AE9a primary leukemia cells.
(G) The knockdown (KD) efficiency of *Tspan13* in *Tet2*$^{-/-}$ (ΔE8–10) MA9 primary leukemia cells as determined by qPCR.
(H) The effect of *Tsapn13* KD on the colony-forming ability of *Tet2*$^{-/-}$ (ΔE8–10) MA9 primary leukemia cells.
(I) The representative colony images of *Tet2*$^{-/-}$ (ΔE8–10) MA9 primary leukemia cells upon *Tspan13* KD.
(J) The effect of *Tsapn13* KD on the colony-forming ability of *Tet2*$^{-/-}$ (ΔE3) NRAS/AE9a primary leukemia cells.
(K) The rescued effect of *Tspan13* KD on *Tet2* deficiency-induced homing. The *in vivo* homing was determined by flow cytometry.
(L) The rescued effect of *Tspan13* KD on Tet2 deficiency (ΔE3)-induced increase of LSC frequency as determined by LDA with NRAS/AE9a primary leukemia cells.
(M) Survival curves of recipient mice transplanted with *Tet2*$^{-/-}$ (ΔE8–10) MA9 primary leukemia cells with or without *Tspan13* KD. n = 5 mice per group. The p values were calculated with a log-rank test (n=5).
(N) The effect of *Tspan13* KD on the engraftment of *Tet2*$^{-/-}$ MA9 cells into the BM and Spleen of recipient mice.
For G, H, J, K, and N, data were presented as mean ± SEM (n=3). *p < 0.05; **p < 0.01; ***p < 0.001; unpaired two-tailed Student's t-test.
See also Figure S6.

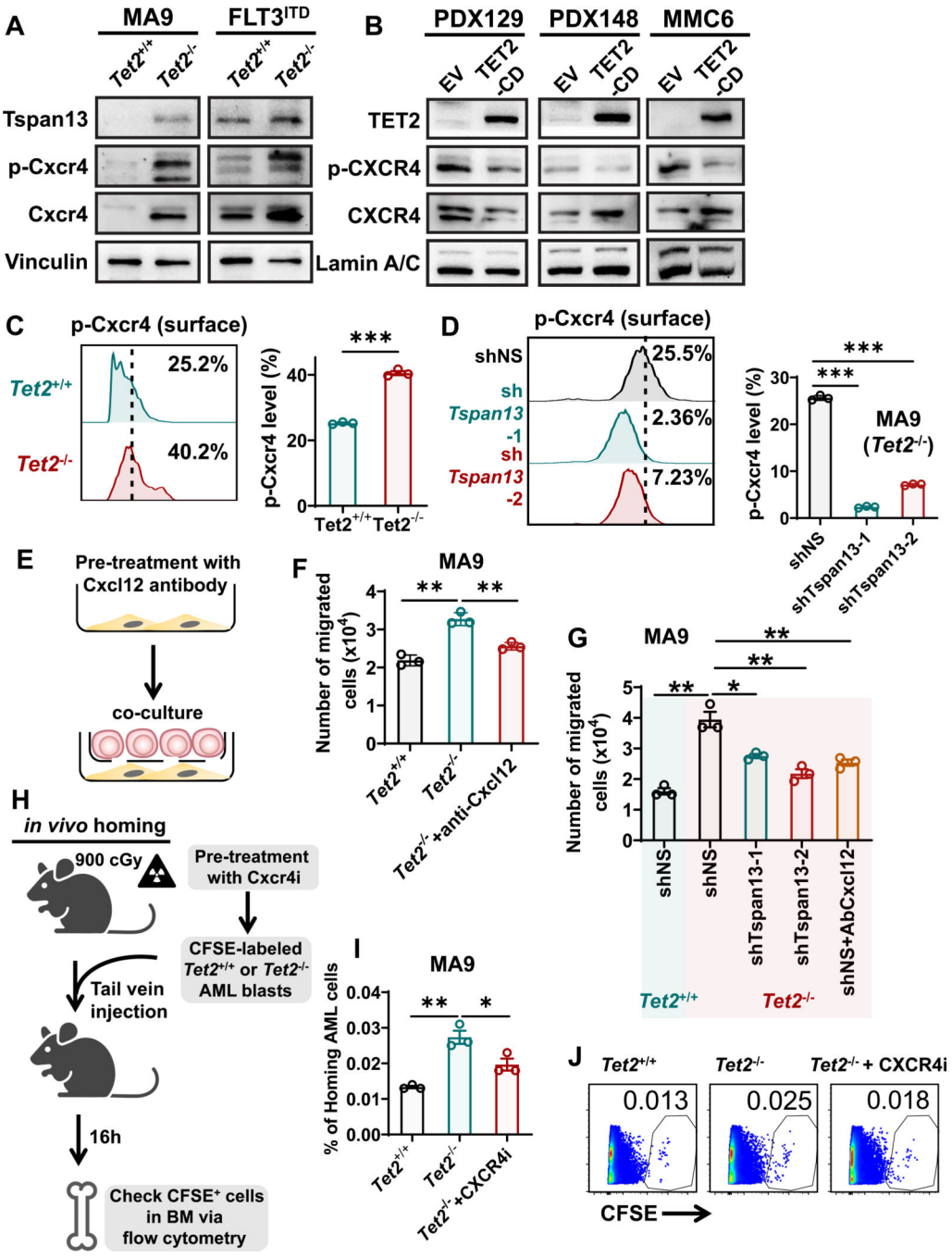


**Figure 6. *Tet2* depletion promotes LSC homing via activating the Tspan13/Cxcr4/Cxcl12 signaling.**

(A) Protein level changes of Tspan13, p-Cxcr4, and Cxcr4 in primary AML cells upon *Tet2* depletion.

(B) Protein level changes of TET2-CD-Flag, p-CXCR4, and CXCR4 in AML PDX cells and cell line (Mono Mac 6, MMC6) upon TET2 overexpression.

(C) Effect of *Tet2* depletion on the expression levels of surface p-Cxcr4 in primary *AE9a/NRAS* AML cells.

(D) Effect of *Tspan13* KD on the expression levels of surface p-Cxcr4 in primary *Tet2*$^{-/-}$ MA9 AML cells.
(E) Schematic outline of transwell assay with stroma cells which were pre-treated with Cxcl12 antibody. The OP9 cells were pretreated with 1μg/ml Cxcl12 antibody for 24–48 hours before co-culture with AML cells.
(F) Effect of Cxcl12 antibody on the migration ability of *Tet2*$^{-/-}$ MA9 primary AML cells.
(G) Effect of *Tspan13* KD and Cxcl12 antibody treatment on the migration ability of *Tet2*$^{-/-}$ MA9 primary AML cells.
(H) Schematic outline of a strategy to evaluate the effect of Cxcr4 inhibitor (Cxcr4i, AMD3100) on the homing. Before transplantation, the MA9 primary AML cells were treated with 0.1mg/ml AMD3100 for 20 hours.
(I-J) Statistical results (I) and representative flow cytometry (J) showing the effect of Cxcr4 inhibition on the homing of *Tet2*$^{-/-}$ primary AML cells.
For C, D, F, G, and I, data were presented as mean ± SEM (n = 3 independent experiments). *p < 0.05, **p < 0.01, ***p < 0.001; unpaired two-tailed Student's t-test.

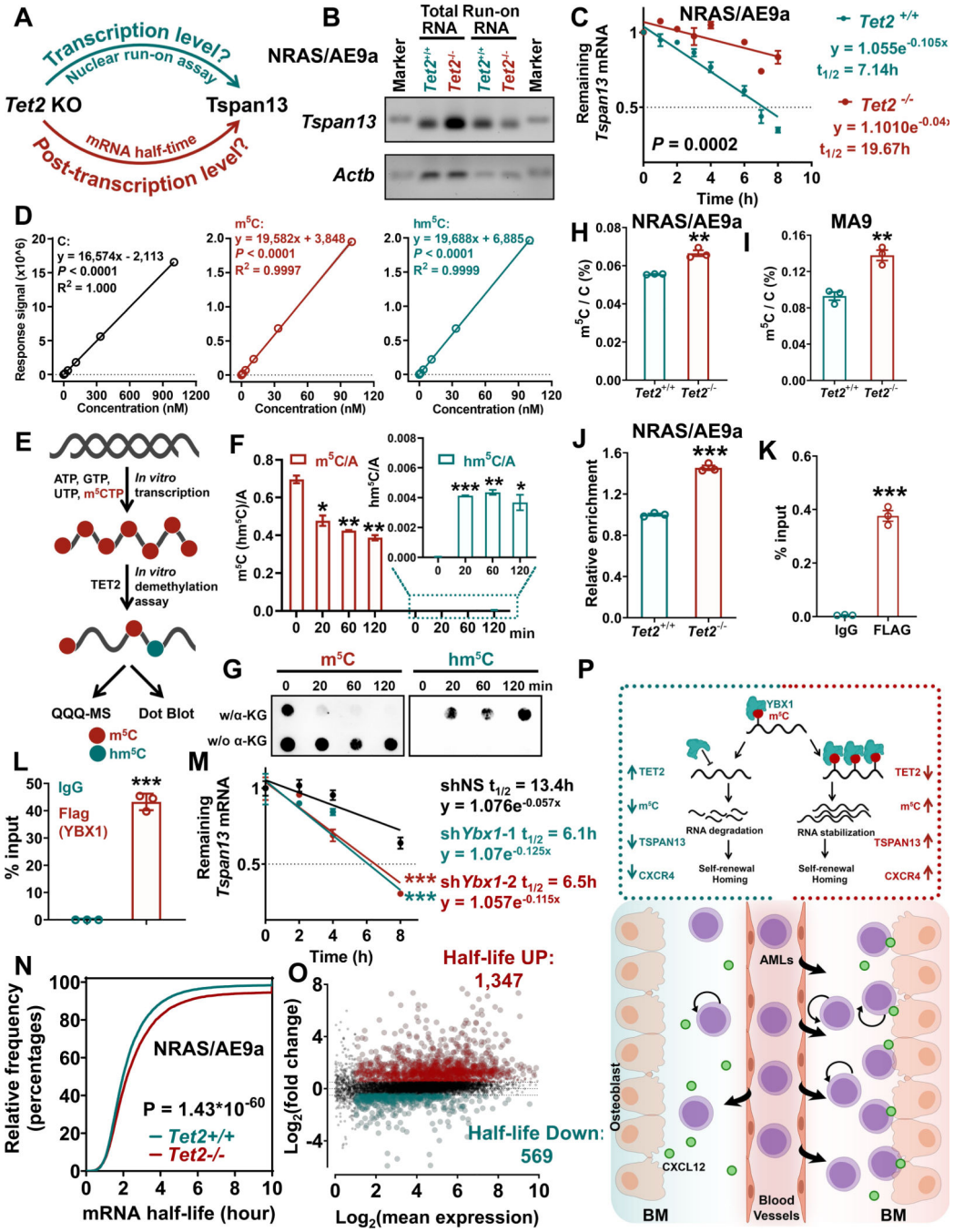


**Figure 7. *Tet2* induces the degradation of *Tspan13* and thus negatively regulates its expression as an mRNA m$^5$C demethylase.**

(A) The possible mechanisms through which Tet2 regulates *Tspan13* expression.

(B) The transcription efficiency of *Tspan13* in *Tet2*$^{+/+}$ and *Tet2*$^{-/-}$ (ΔE3) NRAS/AE9a leukemia cells as determined by nuclear run-on assay.

(C) Effect of Tet2 deficiency (ΔE3) on *Tspan13* mRNA stability in primary NRAS/AE9a AML cells.

(D) The calibration curves of cytosine (C), m$^5$C, and hm$^5$C standards as determined by QQQ-MS.

(E) Scheme of the *in vitro* transcription assay as well as the *in vitro* (cell-free) demethylation assay with TET2 protein and $m^5C$-modified *TSPAN13* mRNA.
(F and G) Assessing the $m^5C$ (left) and $hm^5C$ (right) level changes in *TSPAN13* mRNA in the *in vitro* demethylation assay with TET2 protein as detected by QQQ-MS (F) or dot blot assays (G).
(H and I) The abundance of $m^5C$ in the poly(A) RNA isolated from NRAS/AE9a (H) and MA9 (I) primary leukemia cells with or without *Tet2* deficiency.
(J) Relative levels of *Tsapn13* mRNA $m^5C$ modification in $Tet2^{+/+}$ and $Tet2^{-/-}$ (ΔE3) NRAS/AE9a primary leukemia cells as determined by gene-specific $m^5C$ qPCR.
(K) The direct interaction between Tet2 protein and *TSPAN13* mRNA as detected by CLIP-qPCR in C1498 AML cells. Here, we overexpressed Flag-tagged Tet2 catalytic domain (CD) and performed CLIP with Flag antibody.
(L) The direct interaction between Ybx1 (Flag-tagged) and *Tspan13* mRNA as detected by CLIP-qPCR in C1498 AML cells.
(M) The effect of *Ybx1* KD on *Tspan13* mRNA stability in C1498 AML cells.
(N) The cumulative distribution function (CDF) plot showing the effect of *Tet2* depletion on global mRNA stabilities in NRAS/AE9a primary leukemia cells.
(O) The MA plot showing the mRNAs with significantly increased stability (Half-life UP; Red) and decreased stability (Half-life Down; Green) in NRAS/AE9a primary leukemia cells upon *Tet2* depletion.
(P) The schematic diagram showing how Tet2 regulates LSC homing and self-renewal via targeting the $m^5C$/TSPAN13/CXCR4 axis in the BM microenvironment.
For C, F, and H-N, data were presented as mean ± SEM (n=3 independent experiments). **p < 0.01, ***p < 0.001; unpaired two-tailed Student's t-test.
See also Figure S7.

## KEY RESOURCES TABLE

| REAGENT or RESOURCE | SOURCE | IDENTIFIER |
|---|---|---|
| **Antibodies** | | |
| Anti-5mC antibody | Active Motif | Cat# 39649, RRID:AB_2687950 |
| Anti-5mC antibody | Abcam | Cat# ab10805, RRID:AB_442823 |
| Anti-5hmC antibody | Active Motif | Cat# 39769, RRID:AB_10013602 |
| Anti-GAPDH antibody | Proteintech | Cat# 10494-1-AP, RRID:AB_2263076 |
| Anti-alpha-Tubulin Antibody | Cell Signaling Technology | Cat# 3873, RRID:AB_1904178 |
| Anti-vinculin Antibody | Santa Cruz Biotechnology | Cat# sc-25336; RRID: AB_628438 |
| Anti-FLAG M2 antibody | Sigma-Aldrich | Cat# F3165; RRID: AB_259529 |
| Normal Mouse IgG control antibody | Millipore | Cat# NI03-100UG, RRID:AB_490557 |
| Rabbit IgG normal antibody | Millipore | Cat# NI01-100UG, RRID:AB_490574 |
| Anti-CXCR4 antibody | Proteintech | Cat# 60042-1-Ig, RRID:AB_2091809 |
| Anti-CXCR4 (phospho Ser339) antibody | GeneTex | Cat# GTX32281, RRID:AB_2887647 |
| Anti-CXCR4 (phospho Ser339) antibody | Thermo Fisher Scientific | Cat# BS-12256R |
| Anti-TSPAN13 antibody | Abbexa | Cat# abx214152 |
| Anti-Lamin A/C | Cell Signaling Technology | Cat# 4777, RRID:AB_10545756 |
| Anti-Mouse CXCR4 PE | BioLegend | Cat# 146505, RRID: AB_2562782 |
| Anti-Human CD45 APC | Thermo Fisher Scientific | Cat# 17-9459-42, RRID: AB_10714837 |
| Anti-Human anti-CD33 PE | Thermo Fisher Scientific | Cat# 12-0339-42, RRID: AB_10855031 |
| Anti-CXCL12 antibody | R&D Systems | Cat# MAB310-100, RRID: AB_2276927 |
| Goat anti-rabbit IgG H&L (HRP) | Abcam | Cat# ab6721; RRID: AB_955447 |
| Goat anti-mouse IgG H&L (HRP) | Abcam | Cat# ab6789; RRID: AB_955439 |
| Anti- mouse CD16/32 | eBioscience | Cat# 14-0161-82, RRID: AB_467133 |
| Anti-mouse CD45.2 FITC | BioLegend | Cat# 109806, RRID:AB_313443 |
| Anti-Mouse Lineage marks eFlour 450 | eBioscience | Cat# 88-7772-72, RRID: AB_10426799 |
| Anti-Mouse c-Kit APC | eBioscience | Cat# 17-1171-83, RRID: AB_469431 |
| Anti-Mouse c-Kit APC-Cy7 | BioLegend | Cat# 135136, RRID:AB_2632809 |
| Anti-Mouse Sca-1 PE | eBioscience | Cat# 12-5981-82, RRID: AB_466086 |
| Anti-Mouse Mac-1 PerCP-Cyanine5.5 | eBioscience | Cat# 45-0112-82, RRID:AB_953558 |
| Anti-Mouse Gr-1 PE | eBioscience | Cat# 12-5931-81, RRID:AB_46604 |
| Anti-Mouse CD34 APC | BioLegend | Cat# 128612, RRID:AB_10553896 |
| Anti-Mouse CD16/32 PE-Cy7 | Thermo Fisher Scientific | Cat# 25-0161-82, RRID:AB_469598 |
| Anti-Mouse CD8 APC | eBioscience | Cat# 17-0083-81, RRID:AB_657760 |
| Anti-Mouse osteopontin PE | R&D Systems | Cat# IC808P, RRID:AB_10643832 |
| Phalloidin, CF647 conjugate | Biotium | Cat# 00041-T |
| 7-AAD | BD Biosciences | Cat# 559925, RRID:AB_2869266 |
| **Bacterial and virus strains** | | |
| Stbl3 E. coli | ThermoFisher | Cat# C7373-03 |

| REAGENT or RESOURCE | SOURCE | IDENTIFIER |
|---|---|---|
| **Chemicals, peptides, and recombinant proteins** | | |
| Hexadimethrine bromide (Polybrene) | Sigma-Aldrich | Cat# H9268; CAS: 28728-55-4 |
| Puromycin dihydrochloride | Sigma-Aldrich | Cat# P8833; CAS: 58-58-2 |
| G418 Sulfate | Thermo Fisher Scientific | Cat# 10131027; CAS: 108321-42-2 |
| L-Glutamine (200mM) | Thermo Fisher Scientific | Cat# 25030-081 |
| Ammonium Chloride Solution | STEMCELL Technologies | Cat# 07850 |
| Sodium Pyruvate (100mM) | Thermo Fisher Scientific | Cat# 11360-070 |
| Insulin, human recombinant zinc solution | Thermo Fisher Scientific | Cat# 12585014 |
| Penicillin Streptomycin | Thermo Fisher Scientific | Cat# 15-140-122 |
| Plasmocin prophylactic | Invivogen | Cat# ant-mpp |
| X-tremeGENE™ HP DNA Transfection Reagent | Roche | Cat# 6366236001 |
| Benzonase | Sigma-Aldrich | Cat# E1014 |
| Phosphdiesterase I | Sigma-Aldrich | Cat# P3243, |
| Alkaline phosphatase | Thermo Fisher Scientific | Cat# EF0651 |
| RIPA Buffer | Sigma-Aldrich | Cat# R0278 |
| Halt Phosphatase Inhibitor Cocktail | Thermo Fisher Scientific | Cat# 78420 |
| Halt Protease Inhibitor Cocktail | Thermo Fisher Scientific | Cat# 78429 |
| 4 × Laemmli Sample Buffer | Bio-Rad | Cat# 1610747 |
| Bio-Rad Protein Assay | Bio-Rad | Cat# 5000006 |
| PageRuler Plus Prestained Protein Ladder | Thermo Fisher Scientific | Cat# 26620 |
| Amersham ECL Prime Western Blotting Detection Reagent | GE Healthcare | Cat# 45-010-090 |
| Pierce™ ECL Western Blotting Substrate | Thermo Fisher Scientific | Cat# PI32106 |
| Fluoroshield with DAPI | Sigma-Aldrich | Cat# F6057 |
| Recombinant mouse IL-3 | PeproTech | Cat# 213-13 |
| Recombinant mouse IL-6 | PeproTech | Cat# 216-16 |
| Recombinant mouse SCF | PeproTech | Cat# 250-03 |
| Recombinant murine GM-CSF | PeproTech | Cat# 315-03 |
| Recombinant Murine IFN-γ | PeproTech | Cat# AF-315-05 |
| Recombinant Mouse IFN-β | R&D SYSTEMS | Cat# 8234-MB-010 |
| ColonyGEL-Mouse Base Medium | Reachbio | Cat# 1201 |
| FastDigest NotI | Thermo Fisher Scientific | Cat# FD0595 |
| FastDigest XbaI | Thermo Fisher Scientific | Cat# FD0684 |
| FastDigest BglII | Thermo Fisher Scientific | Cat# FD0083 |
| FastDigest XhoI | Thermo Fisher Scientific | Cat# FD0694 |
| FastDigest KspAI | Thermo Fisher Scientific | Cat# FD1034 |
| CFSE | eBioscience | Cat# 65-0850-84 |
| Actinomycin D | Sigma-Aldrich | Cat#A9415; CAS: 50-76-0 |
| L-Ascorbic acid | Sigma-Aldrich | Cat# A0278, CAS: 50-81-7 |
| DL-Dithiothreitol solution | Sigma-Aldrich | Cat# 3483-12-3; CAS: 3483-12-3 |

| REAGENT or RESOURCE | SOURCE | IDENTIFIER |
|---|---|---|
| α-Ketoglutaric acid | Sigma-Aldrich | Cat# 75890, CAS: 328-50-7 |
| Adenosine-5 Triphosphate (ATP) | New England Biolabs | Cat# P0756S |
| PMA | Sigma-Aldrich | Cat# P1585, CAS: 16561-29-8 |
| Ionomycin | Sigma-Aldrich | Cat# I9657, CAS: 56092-81-0 |
| Propidium Iodide | Sigma-Aldrich | Cat# P4170; CAS: 25535-16-4 |
| NEBNext Magnesium RNA Fragmentation Module | New England Biolabs | Cat# E6150S |
| 0.5M EDTA | Thermo Fisher Scientific | Cat# 15575020 |
| Formaldehyde solution | Sigma-Aldrich | Cat# F8775, CAS: 50-00-0 |
| 1M Tris-HCl, pH 8.0 | Invitrogen | Cat# 15568025 |
| 1 M Tris-HCI Buffer, pH 7.5 | Thermo Fisher Scientific | Cat# 15567027 |
| Sodium Chloride Solution, 5M | Sigma-Aldrich | Cat# S6546 |
| Paraformaldehyde Solution | Fisher scientific | Cat# AAJ19943K2 |
| IC Fixation buffer | eBioscience | Cat# 00-8222-49 |
| Permeabilization Buffer (10X) | Thermo Fisher Scientific | Cat# 00-8333-56 |
| Wright-Giemsa Stain | Polysciences | Cat# 24985 |
| Wright-Giemsa Stain/Buffer | Polysciences | Cat# 24984 |
| Pierce Protein A/G Magnetic Beads | Thermo Fisher Scientific | Cat# 88803 |
| D-Luciferin Firefly, potassium salt | Goldbio | Cat# LUCK; CAS: 115144-35-9 |
| Platinum™ SuperFi II DNA Polymerase | Thermo Fisher Scientific | Cat# 12361010 |
| Recombinant TET2 protein | Active Motif | Cat# 31418 |
| RNaseOUT Recombinant Ribonuclease Inhibitor | Thermo Fisher Scientific | Cat# 10777019 |
| T4 DNA ligase | Fisher Scientific | Cat# M0202S |
| Biotin-16-UTP | Sigma-Aldrich | Cat# 11388908910 |
| 5-methylcytidine-5’-triphosphate (5mCTP) | TriLink Biotechnologies | Cat# N-1014-1 |
| 5-Hydroxymethylcytidine | Carbosynth | Cat# NH35521, CAS: 19235-17-7 |
| 5-Methyl-2’-deoxycytidine | Cayman Chemical Company | Cat# 16166, CAS: 838-07-3 |
| Cytidine | Cayman Chemical Company | Cat# 29602, CAS: 65-46-3 |
| Guanosine | Cayman Chemical Company | Cat# 27702, CAS: 118-00-3 |
| 5-(Hydroxymethyl)-2’-deoxycytidine | Cayman Chemical Company | Cat# 18162, CAS: 7226-77-9 |
| 5-(Hydroxymethyl)-2’-deoxycytidine-d3 | Toronto Research Chemicals | Cat# H946632, CAS: 7226-77-9 |
| 5-Hydroxymethylcytidine-13C,D2 | Toronto Research Chemicals | Cat# H947092, CAS: 19235-17-7 |
| 5-Methyl-2’-deoxy Cytidine-d3 | Toronto Research Chemicals | Cat# M295902; CAS: 1160707-78-7 |
| Guanosine-5’,5″-d2 Monohydrate | Toronto Research Chemicals | Cat# G837915, CAS: 478511-34-1 |
| DNase I, RNase-free (1 U/μL) | Thermo Fisher Scientific | Cat# EN0521 |
| TURBO DNase | Thermo Fisher Scientific | Cat# AM2239 |

| REAGENT or RESOURCE | SOURCE | IDENTIFIER |
|---|---|---|
| RNase A (DNase free) | Thermo Fisher Scientific | Cat# EN0531 |
| Proteinase K | Thermo Fisher Scientific | Cat# EO0492 |
| Dynabeads M-280 streptavidin | Thermo Fisher Scientific | Cat# 11205D |
| TRIzol™ Reagent | Thermo Fisher Scientific | Cat# 15596-018 |
| AMD3100 | Selleckchem | Cat# S3013 |
| **Critical commercial assays** | | |
| Oligo Clean & Concentrator kit | Zymo Research | Cat# D4061 |
| Cell Counting Kit 8 | Dojindo | Cat# CK04 |
| Click-iT EdU Alexa Fluor 647 Flow Cytometry Assay Kit | Thermo Fisher Scientific | Cat# C10424 |
| EdU Proliferation Kit (iFluor 488) | Abcam | Cat# ab219801 |
| In-Fusion HD Cloning Plus CE Cat# | Takara | Cat# 638916 |
| PCR Mycoplasma Detection Kit | Applied Biological Materials | Cat# G238 |
| DNeasy Blood & Tissue Kit | QIAGEN | Cat# 69506 |
| CD117 MicroBead Kit, mouse | Miltenyi Biotec | Cat# 130-091-224 |
| Lineage Cell Depletion Kit | Miltenyi Biotec | Cat#130-090-858 |
| Pan T Cell Isolation Kit II | Miltenyi Biotec | Cat# 130-095-130 |
| RNA Clean & Concentrator-5 | Zymo Research | Cat# R1014 |
| ChIP DNA Clean & Concentrator kit | Zymo Research | Cat# D5201 |
| RNeasy mini kit | Qiagen | Cat# 74104 |
| QIAGEN Plasmid Mini Kit | Qiagen | Cat# 27104 |
| PolyATract mRNA isolation system IV | Promega | Cat# Z5310 |
| QuantiTect Reverse Transcription Kit | Qiagen | Cat# 205314 |
| Maxima SYBR Green qPCR Master Mix | Thermo Fisher Scientific | Cat# K0253 |
| SuperScript™ III First-Strand Synthesis System | Invitrogen | Cat# 18080051 |
| MEGAscript™ T7 kit | Invitrogen | Cat# AM1333 |
| MEGAclear™ Transcription Clean-Up Kit | Invitrogen | Cat# AM1908 |
| EZ RNA Methylation Kit | Zymo Research | Cat# R5002 |
| **Deposited data** | | |
| RNA-seq (Raw and analyzed data) | This manuscript | GSE206488 |
| mRNA half-life profiling & mRNA Bis-seq | This manuscript | GSE231330 |
| **Experimental models: Cell lines** | | |
| C1498 | A gift from Dr. Marcin Kortylewski | N/A |
| Mono Mac 6 | DSMZ | Cat# ACC 124; RRID: CVCL_1426 |
| OP9 | ATCC | Cat# CRL-2749; RRID: CVCL_4398 |
| HEK293T | ATCC | Cat# CRL-3216; RRID: CVCL_0063 |
| **Experimental models: Organisms/strains** | | |
| NRGS mouse | The Jackson Laboratory | Cat# JAX:024099; RRID: IMSR_JAX:024099NCI |

| REAGENT or RESOURCE | SOURCE | IDENTIFIER |
|---|---|---|
| NCI B6-Ly5.1/Cr mouse | Charles river | Cat# CRL:564; RRID: IMSR_CRL:564 |
| B6(Cg)-*Tet2*$^{tm1.2Rao}$/J (ΔE8-10) | The Jackson Laboratory | Cat# 023359 RRID:IMSR_JAX:023359 |
| Tet2$^{-/-}$ (ΔE3) | A gift from Dr. Mingjiang Xu | N/A |
| **Oligonucleotides** | | |
| Primers for Real-time PCR, see Table S1 | Integrated DNA Technologies (IDT) | N/A |
| **Recombinant DNA** | | |
| pcDNA3-TET2-CD | A gift from Dr. Yue Xiong | N/A |
| pMSCV-PIG-NRAS$^{G12D}$ | This paper | N/A |
| pMSCV-Neo-AF9a | This paper | N/A |
| pMSCV-Neo-PML-RARA | This paper | N/A |
| pMSCV-Neo-MLL AF9 | A gift from Dr. Michael Thirman | N/A |
| pcDNA3-Tet2 | Wang et al.[70] | RRID:Addgene_60939 |
| pMSCV-Flt3-ITD-Y591F/Y919F | Kazi et al.[71] | RRID:Addgene_74499 |
| pMSCV-PIG-3×FLAG-NotI | This paper | N/A |
| pMSCV-Neo-3×FLAG | This paper | N/A |
| pMSCV-PIG-3×FLAG-Tspan13 | This paper | N/A |
| pMSCV-PIG-3×FLAG-Ybx1 | This paper | N/A |
| pMSCV-PIG-3XFLAG-mTet2 CD | This paper | N/A |
| pCDH-3×FLAG-TET2 CD | This paper | N/A |
| pLenti CMV Puro LUC (w168-1) | Campeau et al.[72] | Cat# Addgene plasmid # 17477; RRID: Addgene_17477 |
| pMD2.G | A gift from Dr. Didier Trono | Cat# Addgene plasmid # 12259; RRID: Addgene_12259 |
| psPAX2 | A gift from Didier Trono | Cat# Addgene plasmid # 12260; RRID: Addgene_12260 |
| pLKO.1 puro | Stewart et al.[73] | Cat# Addgene plasmid # 8453; RRID: Addgene_8453 |
| pLKO.1-shTspan13-1 | This paper | N/A |
| pLKO.1-shTspan13-2 | This paper | N/A |
| pLKO.1-shYbx1-1 | This paper | N/A |
| pLKO.1-shYbx1-2 | This paper | N/A |
| pMSCV-MLL-AF9-Neo | A gift from Dr. Michael Thirman | N/A |
| pCL-Eco | Naviaux et al.[74] | Cat# Addgene plasmid # 12371; RRID: Addgene_12371 |
| **Software and algorithms** | | |
| GraphPad Prism | GraphPad | https://www.graphpad.com/scientific-software/prism/ |
| GelAnalyzer | GelAnalyzer | http://www.gelanalyzer.com/ |
| RSEM-1.2.31 | Li and Dewey[75] | https://deweylab.github.io/RSEM/ |

| REAGENT or RESOURCE | SOURCE | IDENTIFIER |
|---|---|---|
| STAR 2.7 | Dobin et al.[76] | https://github.com/alexdobin/STAR |
| igv-2.3.72g | Thorvaldsdottir et al.[77] | http://software.broadinstitute.org/software/igv/ |
| GSEA 4.2.0 | Subramanian et al.[78] | https://www.gsea-msigdb.org/gsea/index.jsp |